Electrochimica Acta 471 (2023) 143360

Contents lists available at ScienceDirect

Electrochimica Acta

journal homepage: www.journals.elsevier.com/electrochimica-acta

Efficient electrochemical nitrogen fixation at iron phosphide (Fe_2P) catalyst in alkaline medium

Beata Rytelewska [a], Anna Chmielnicka [a], Takwa Chouki [b], Magdalena Skunik-Nuckowka [a], Shaghayegh Naghdi [c], Dominik Eder [c], Aleksandra Michalowska [a], Tomasz Ratajczyk [a], Egon Pavlica [d], Saim Emin [b], Yongsheng Fu [e], Iwona A. Rutkowska [a,*], Pawel J. Kulesza [a,*]

[a] Faculty of Chemistry, University of Warsaw, Pasteura 1, Warsaw 02-093, Poland
[b] Materials Research Laboratory, University of Nova Gorica, Ajdovscina 5270, Slovenia
[c] Institut für Materialchemie, Technische Universität Wien, Getreidemarkt 9, Vienna 1060, Austria
[d] Laboratory of Organic Matter Physics, University of Nova Gorica, Vipavska Cesta 13, Nova Gorica SI-5000, Slovenia
[e] School of Chemistry and Chemical Engineering, Nanjing University of Science and Technology, Nanjing 210094, China

ARTICLE INFO

Keywords:
Nitrogen reduction
Alkaline medium
Iron phosphide catalyst
Ammonia
Electrochemical determinations
Electroanalytical control experiments

ABSTRACT

A catalytic system based on iron phosphide (Fe_2P) has exhibited electrocatalytic activity toward N_2-reduction reaction in alkaline medium (0.5 mol dm^{-3} NaOH). Based on voltammetric stripping-type electroanalytical measurements, Raman spectroscopic and spectrophotometric data, it can be stated that the Fe_2P catalyst facilitates conversion of N_2 to NH_3, and the process is fairly selective with respect to the competing hydrogen evolution. A series of diagnostic electrocatalytic experiments (utilizing platinum nanoparticles and HKUST-1) have been proposed and performed to control purity of nitrogen gas and to probe presence of potential contaminants such as ammonia, nitrogen oxo-species and oxygen. On the whole, the results are consistent with the view that the interfacial reduced-iron (Fe^0) centers, while existing within the network of P sites, induce activation and reduction of nitrogen, parallel to the water splitting (reduction) to hydrogen. It is apparent from Tafel plots and impedance measurements that mechanism and dynamics of nitrogen reduction depends on the applied electroreduction potential. The catalytic system exhibits certain tolerance with respect to the competitive hydrogen evolution and gives (during electrolysis at -0.4 V vs. RHE) the Faradaic efficiency, namely, the selectivity (molar) efficiency, toward production of NH_3 on the level of 60%. Under such conditions, the NH_3-yield rate has been found to be equal to 7.5 μmol cm^{-2} h^{-1} (21 μmol m^{-2} s^{-1}). By referring to classic concepts of electrochemical kinetic analysis, the rate constant in heterogeneous units has been found to be on the moderate level of 1-2*10^{-4} cm s^{-1} (at -0.4 V). The above mentioned iron-phosphorous active sites, which are generated on surfaces of Fe_2P particles, have also been demonstrated to exhibit strong catalytic properties during reductions of other electrochemically inert reactants, such as oxygen, nitrites and nitrates.

1. Introduction

Ammonia (NH_3) is manufactured on a large scale world-wide and is used to produce fertilizers, plastics, fibers, explosives, nitric acid, and intermediates for dyes and pharmaceuticals. Furthermore, ammonia has received much attention an alternative fuel for vehicles and, as carbon-free hydrogen carrier, it can act as a potential energy storage medium [1–3]. Ammonia is mainly produced via the Haber-Bosch synthetic process [4],

$$N_2 + 3H_2 \rightarrow 2NH_3 \quad (1)$$

in which nitrogen from the air is combined with hydrogen under extremely high pressures (at least 100−300 bar) and fairly high temperatures (400−500°C, or lightly higher). Heterogeneous catalysts (based mostly on iron) enable the reaction to be carried out at reasonably high (thermodynamically-justified) temperatures, whereas the removal of ammonia from the batch as soon as it is formed ensures that equilibrium favoring the product formation is maintained. While being the most efficient for the fixation (reduction) of nitrogen, the Haber-Bosch synthesis is the basic process of chemical industry. But it

* Corresponding authors.
E-mail addresses: ilinek@chem.uw.edu.pl (I.A. Rutkowska), pkulesza@chem.uw.edu.pl (P.J. Kulesza).

https://doi.org/10.1016/j.electacta.2023.143360
Received 10 June 2023; Received in revised form 5 October 2023; Accepted 14 October 2023
Available online 18 October 2023

depends on plentiful supplies of energy and is believed to contribute to a buildup of reactive nitrogen in the biosphere, causing an anthropogenic disruption to the nitrogen cycle [5] Furthermore, the requirement of the enormous supply of hydrogen, which is generated by fossil fuels, leads to significant carbon dioxide emissions. Consequently, there is a growing interest in sustainable production which include electrolytic approaches with renewable energy sources.

Electrocatalytic N_2-reduction under ambient-condition is considered to be a tempting strategy to synthesize ammonia while alleviating greenhouse emissions and reducing environmental pollution [6–10]. In the reaction, nitrogen is reduced to ammonia in an aqueous environment at the cathode using six-electrons and water as the source of hydrogen:

$$N_2 + 6H_2O + 6e^- \rightarrow 2NH_3 + 6OH^- \quad (2)$$

But electroreduction is a sluggish multi-step process and requires breaking the strong (941 kJ mol^{-1}) triple (N≡N) bond in a stable N_2 molecule [11–13]. The major scientific challenges for the N_2-to-NH_3 conversion include the need of activation through sufficiently strong (but not irreversible) adsorption of nitrogen molecule at the catalytic interface. But electrocatalysts are typically more active toward hydrogen evolution than ammonia production. Among other issues is the long-term stability that does not limit the practical use and technological commercialization of N_2-fixation catalysts at mild conditions [14–17]. In addition to the choice of a functional electrocatalyst, consideration of a proper electrolyte is also critical to achieve the desired performance.

There is a need to develop electrocatalytic systems for N_2-reduction reaction (N_2RR) that are optimized for activity and durability. Representative catalytic materials include a variety of systems covering noble-metal catalysts [18–21], noble-metal-free alternatives [22–37], and transition-metal-based materials with the abundant d-orbital electrons and unoccupied orbitals capable of the activation of strong N≡N triple bond [38,14]. Among transition metals, promising results have been reported with the iron-group (Fe, Co, Ni and Cu) [39,40] electrocatalysts. Such systems can also be considered as cocatalysts or additives, as well as in a form of oxides, hydroxides, nitrides, sulfides and phosphides, which are known to exhibit to exhibit reasonable stability and remarkable catalytic activation. Obviously many other materials [41–43], including distinct metals, alloys [44], enzymes [45] and metal nitrides [46] have been tested for N_2RR but, in most cases they still suffer from low selectivity and activity for this reaction.

Having in mind, the activity of the enzyme nitrogenase [47], it is reasonable to expect that iron (Fe) sites may interact strongly with nitrogen and enhance both the adsorption and activation of N_2 molecules. The fact that Fe element is placed in the middle of the lighter transition metal elements within the periodic table suggests the existence of unoccupied d orbitals capable to act as both electron-acceptor and electron-donors [48]. For example, the graphene-embedded FeN_3-type centers exhibit catalytic properties for nitrogen fixation [49]. Also Fe-ionic sites coordinated within C_3N_4 network can activate the N_2 molecule effectively [50]. Theoretical predictions [51] imply that Fe-doped monolayer of black phosphorous, phosphorene, would function as effective catalytic system, in which single atom Fe centers, while cooperating or interacting with P sites activate the inert N≡N triple bond and induce N_2-reduction to NH_3. Being inspired by this report and our recent observations concerning the electrocatalytic activity of iron phosphides toward reduction of nitrates to ammonia [52], we have concentrated on the latter class of compounds.

Transition metal phosphides, in particular Fe-based metal phosphides (FeP, Fe_2P, FeP_2, Fe_3P) [53,54], have been widely applied in photocatalysis [55,56], electrocatalysis [57–62], in the development of sensors [63] and batteries [58,64] due to their unique catalytic properties, long stability, and fairly high conductivity. The presence of phosphorus can lead to the "weak ligand" effect upon the formation of metal-P bonds in metal phosphides [65]. It has been postulated that, in a case of Fe-based metal phosphides, the vacant 3***d***-orbital and the 3***p***-lone-pair electrons of P-atoms can modify the surface charge densities characteristic of Fe atoms [66]. The transition metal phosphides, in which the nanostructured catalytic iron sites could exist, are promising low-cost candidates for electrocatalytic reduction reactions [67–73]. Among important features is existence of the charge transfer effect, M(δ^+) → P(δ^-), which permits reversible formation of the adsorbed hydrogen atoms (H) at the catalytic interface [67,70,74]. The systems' good conductivity [75] is also advantageous.

In the present study, we report the successful electrocatalytic reduction of nitrogen (N_2) in 0.5 mol dm^{-3} NaOH using of iron phosphide activated at 300°C, namely in a form of Fe_2P. At ambient conditions, Fe_2P is hexagonal with iron atoms at two, tetrahedral and pyramidal, nonequivalent sites surrounded by four and five phosphorous atoms, respectively [76,78]. For example, the Fe^{1+} sites, which are bonded to four equivalent P^{3-} atoms, form a mixture of distorted edge and corner-sharing FeP_4 tetrahedra. Judging from the stoichiometry of Fe_2P, both Fe^{I} and Fe^{II} ionic sites are expected to exist at open-circuit potential (i.e., in the initial state of an electrochemical experiment). The physicochemical identity and structure of the electrocatalytic interface polarized negatively toward reduction of N_2 and exposed to liquid electrolyte would obviously be different than that characteristic of the initial state. Our observations are consistent with the view that catalytic electroreduction of N_2 is induced by pre-reduced Fe^0 atoms generated from Fe-ionic sites of Fe_2P catalyst but only on its surface. We have also considered Tafel plots, impedance measurements and classic concepts of kinetic electroanalysis to comment on mechanism and dynamics of nitrogen reduction. Identification of the NRR products have been addressed using Raman spectroscopy, as well as using the *in-situ* electroanalytical detection approach based on probing the electrooxidation of NH_3 to nitrogen (N_2) at the extra working electrode modified with Pt nanoparticles. Supplementary diagnostic experiments have also been carried out to control purity of nitrogen gas and to identify potential contaminants. To comment on general catalytic activity of Fe_2P during electroreductions in alkaline medium, we have performed additional comparative measurements using such redox probes as O_2, CO_2, NO_3^- and NO_2^-.

2. Experimental

Chemical reagents were analytical grade materials. Iron pentacarbonyl (>99.99%, $Fe(CO)_5$), oleylamine (70%, OLA), ethanol (98%, EtOH), acetone (95%) and 5wt% Nafion® perfluorinated resin solution were obtained from Sigma-Aldrich. Platinum black nanoparticles, triphenylphosphine (99%, TPP), and squalene (98%, SQ) were purchased from Alpha Aesar. Sodium hydroxide and sulfuric acid (95%) were bought from POCh (Gliwice, Poland).

All chemicals were analytical grade materials and were used as received. Solutions were prepared from the deionized (Millipore Milli-Q) water. They were deoxygenated by bubbling with ultrahigh purified argon. Experiments were carried out at room temperature (22 ± 2°C).

All electrochemical measurements were performed using a CH Instruments (Austin, TX, USA) Model 760D workstation in three electrodes configuration. The glassy carbon working electrode was in a form of the disk of geometric area, 0.071 cm^2. As a rule, the surface of the electrode was pre-cleaned and pretreated by polishing with alumina on (Buhler polishing cloth). The reference electrode was Ag/AgCl, KCl (saturated) electrode, and the gold electrode (immersed in a glass Luggin capillary) was used as the counter electrode. All potentials reported here were recalculated and expressed vs. RHE.

The synthesis of iron phosphides was performed using a modified solvothermal synthesis procedure described earlier [41,72,73]. In particular, to obtain Fe_2P (which is mostly considered in the present work) 0.6 g $Fe(CO)_5$, 3.14 g TPP as precursor, 10 ml OLA, and 1.0 ml SQ were introduced into a 100 ml three-neck flask (under Ar-atmosphere)

and heated to 150°C (ramp tare: 10°C min^{-1}) until the TPP was dissolved. The temperature was further increased gradually and, finally, was held at 450°C for 15 min. After cooling down the suspension to 50°C, the Fe_2P particles were isolated by adding a mixture of solvents (ethanol/acetone, v/v 1:1). Later, the product was subjected to centrifugation at 8000 rpm for 5 min and, finally, the Fe_2P product was isolated as a solid material. The specific surface area (135 m^2 g^{-1}) of F_2P powder sample was recorded using N_2 adsorption at 77 K (Autosorb iQ-XR from Quantachrome/Anton Paar).

Unless otherwise stated, the Fe_2P catalytic material was introduced through rubbing it onto the glassy carbon electrode surface. The loading of Fe_2P on the electrode surface, ca. 4.9 mg cm^{-2}, was determined by careful weighting of pristine and modified electrodes using microbalance.

As a rule, the films were over-coated and stabilized with ultrathin layers of Nafion polyelectrolyte by depositing 1 μm^3 of the Nafion solution (prepared by introducing 5 wt% of the commercial Nafion solution into ethanol at the 1 to 10 volumetric ratio).

The catalytic materials were first pretreated in the deaerated 0.5 mol dm^{-3} NaOH electrolyte by subjecting them to repetitive potential cycling by subjecting them to repetitive potential cycling (in the range from -0.50 to 0.80 V vs. RHE) at 10 mV s^{-1} for 20 min. Before the actual electrocatalytic experiments were performed, the electrodes were conditioned by potential cycling (4 full potential cycles at 10 mV s^{-1}) in the potential range from -0.50 to 0.80V (vs. RHE) in the N_2-saturated solution of 0.5 mol dm^{-3} NaOH. Before each representative voltammogram was recorded, the working electrode was kept for 20 s ("quiet time") at the starting potential.

Identification of N_2RR product deposited on electrode surfaces has been achieved using Raman spectroscopy. The spectra were measured using a Horiba Jobin-Yvon Labram HR800 spectrometer coupled with a confocal Olympus BX40 microscope with a long distance 50x objective. The Raman spectrometer was equipped with: a Peltier-cooled CCD detector (1024 × 256 pixels), a 600 grove per mm holographic grating, while a He-Ne laser provided the excitation radiation with a wavelength of 532 nm.

Detection of N_2RR products has also been performed electrochemically using glassy carbon electrode modified with iron phosphide under chronoamperometric conditions upon application of the constant potential of -0.40V vs. RHE. During this process, the second glassy carbon working electrode, which was modified with Pt nanoparticles (loading 100 μg cm^2) was used for detection of reaction products. The platinum nanoparticles were first pre-treated in the deaerated 0.5 mol dm^{-3} H_2SO_4 electrolyte by subjecting them to repetitive potential cycling (in the range from 0.04 to 1.04V vs. RHE) at 10 mV s^{-1} for 30 min. Before and after electrolysis voltammetric patterns of platinum nanoparticles were recorded in deoxygenated 0.5 mol dm^{-3} NaOH in the potential range from 0.15 to 1.25V (vs. RHE). The reference electrode was the silver chloride electrode (Ag/AgCl), and the gold electrode was used as the counter electrode.

SEM images of the samples were obtained with field emission SEM Zeiss Merlin, operating at 3 keV beam energy, using secondary electron detectors. TEM Zeiss Libra 120 was also used to capture transmission images, with 120 keV beam. Mean atomic content of the samples was measured utilizing EDS detector Bruker Quantax 400, conjugated with the scanning microscope. The following stoichiometries, $Fe_{1.9}P$, $Fe_{1.0}P$, and $Fe_{2.7}P$ (Fe- determination uncertainty, ±0.03) were obtained for Fe_2P, FeP, and Fe_3P, respectively.

X-ray diffraction (XRD) patterns were measured with MiniFlex 600 W (Rigaku) diffractometer with Cu-Kα radiation.

3. Results and discussion

3.1. Physicochemical characteristics of iron phosphides in alkaline medium

Basic physicochemical characterization of FeP, Fe_2P, and Fe_3P catalysts was provided in our previous publication [72]. The cyclic voltammograms of (a) FeP, (b) Fe_2P, and (c) Fe_3P films (deposited on glassy carbon), which are illustrated in Fig. 1A and 1B, have been recorded in argon-saturated 0.5 mol dm^{-3} NaOH. During cathodic scans starting from 0.8 V down to -0.6 V, the hydrogen evolution reduction currents have appeared at about -0.2 V and have risen sharply at about -0.35 V for all iron phosphide samples studied (Fig. 1B). In other words, the voltammetric responses of all samples studied are comparable. In the potential range from 0.5 to -0.2 V, sets of relatively small and drawn-out cathodic and anodic peaks appear in all cases at similar potentials; they shall be correlated with the electroactivity of iron component of iron phosphide deposits. The respective electrochemical responses are enlarged in Fig. 1A. Because processes of hydrogen evolution (which is typically induced by metallic iron sites) are initiated at ca. -0.2 V, i.e. soon after the small cathodic peaks are developed, it is reasonable to expect that the systems' redox transitions observed below -0.2 V involve generation of the fully reduced iron sites at the iron phosphide surfaces. It is likely that, once Fe^0 sites are generated at the surfaces of Fe_2P catalytic particles, the system's hexagonal structure (with iron atoms tetrahedrally or pyramidally coordinated phosphorous) is largely reorganized. Having in mind that experiments are performed in strong alkaline medium (0.5 mol dm^{-3} NaOH), the sets of voltammetric peaks appearing in the potential range from 0.5 to -0.2 V (Fig. 1A) reflect redox

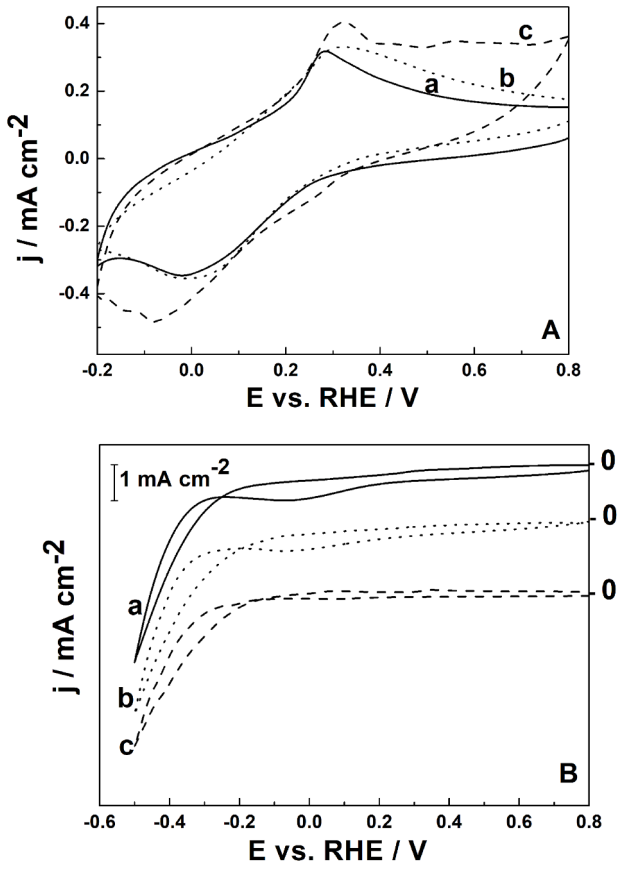

Fig. 1. Cyclic voltammetric responses (recorded at 10 mV s^{-1}) for (**a**) FeP, (**b**) Fe_2P, and (**c**) Fe_3P films (deposited on glassy carbon) in argon-saturated 0.5 mol dm^{-3} NaOH illustrated in two potential ranges: (**A**) from 0.8 to -0.2 V, and (**B**) from 0.8 to -0.5 V.

transitions between iron (most likely Fe^{III} and Fe^{II}) hydroxy species existing in the phosphorous-rich environment.

Despite the fact that iron ions existing in FeP, Fe_2P and Fe_3P have different oxidation states, their reduction to Fe^0 would require three-electrons per iron phosphide molecule. For example, by considering the charge under the Fe_2P reduction peak (Fig. 1A, Curve b), which has been approximated against the extrapolated baseline, and by using Faraday equation, it can be estimated that approximately only $2*10^{-8}$ mol cm^{-2} of Fe_2P units undergo Fe^{III}/Fe^{II} redox transitions (i.e., it is electroactive) at the interface. Simple comparison to the loading of Fe_2P on the glassy carbon electrode surface (ca. 4.9 mg cm^{-2}, what is equivalent to ca. $3.4*10^{-5}$ mol cm^{-2} of Fe_2P) implies that only less than 0.1 molar% of Fe_2P catalyst is electroactive. Obviously, the latter result is likely to be underestimated because separation of charges originating from the surface redox reactions from the background responses also covering Fe_2P capacitive charging/discharging phenomena (Fe_2P surface area, 135 m^2 g^{-1}) is not precise. Nevertheless, the active iron (Fe^0) catalytic sites, which are generated upon reduction of the electroactive iron sites existing on surfaces of Fe_2P particles would constitute very small fraction of the catalytic material. It is reasonable to expect that the bulk rigid structure of Fe_2P is largely retained (it contributes only to the background capacitive currents) while the interfacial Fe^0 catalytic centers are formed. It is commonly accepted that the surface electrochemical response of $1\text{-}2*10^{-10}$ mol cm^{-2} is characteristic of the monolayer-type electroactivity; thus, the value of $2*10^{-8}$ mol cm^{-2} would imply that roughly 100-200 monolayers of iron sites (on Fe_2P submicrometer particles) would undergo transformation to generate Fe^0 catalytic centers. Formation of Fe^0 implies thorough structural reorganization of Fe_2P surfaces (but not of the bulk material) leading to Fe-P bond breaking and separation of iron and phosphorous sites. It cannot be excluded that the resulting catalytic interface may function in an analogous manner to the theoretically predicted system of Fe-doped monolayer phosphorene [51] in which iron catalytic sites, while cooperating with P, are postulated to activate the inert triple bond in N_2 to drive reduction to NH_3.

Fig. 2A illustrates the XRD pattern of the synthesized Fe_2P catalyst recorded upon its activation at 450°C. As before [72], all peaks are assigned to the hexagonal phase characteristic of Fe_2P (*P*62*m*, PDF♯ 1008826). The following Rietveld refined crystal parameters have been found for Fe_2P: $a = b = 0.5910 \pm 0.00070$ nm, and $c = 0.3543 \pm 0.00040$ nm. They are consistent with literature data [72], even with the parameters of Fe_2P single crystals [77].

We previously reported transmission electron microscopic data [72] clearly indicating that Fe_2P is composed of distinct nanostructures, such as nanospheres, nanocubes, and nanorods ranging in sizes from 8 to 15 nm. Microscopic examination (Fig. 2B) of Fe_2P catalysts following subjecting them to voltammetric potential cycling (as for Fig. 1B) implies that Fe_2P nanostructures undergo agglomeration to form submicro-structures. Formation of rather amorphous, porous but fairly thick Fe_2P deposits is particularly apparent from scanning electron microscopic examination of the respective catalytic films on glassy carbon (Fig. 2C).

3.2. *Electrocatalytic properties of Fe_2P*

Fig. 3A illustrates voltammetric responses of the Fe_2P system recorded both in the presence (solid line, solution saturated with N_2), and in the absence of nitrogen (dashed line; solution saturated with Ar). Here the N_2RR currents are definitely higher (solid line), namely they differ significantly from the background response recorded in the absence of nitrogen (dashed line). The result is consistent with reasonably sound selectivity (vs. hydrogen evolution) and appreciable activity of Fe_2P toward N_2RR.

It is apparent from Fig. 3A that both hydrogen evolution and N_2RR appear in the same potential range where iron sites are expected to be in the reduced state (Fe^0), thus inducing reversible formation of the adsorbed hydrogen (H) atoms [67,70,74] (e.g., via interfacial water splitting in alkaline electrolyte: $H_2O + e^- \rightarrow *H + OH^-$ [79]) and activation of the N_2 molecules (to form $*N_2$ radicals). In alkaline medium, these monoatomic H-atom adsorbates (or *H radicals) are not anticipated to combine with water molecules to form H_3O^+ ions but, more likely, the hydrogenation of $*N_2$ (i.e., nitrogen molecule activated at Fe^0 sites) leading to the dissociative adsorption is triggered by water splitting: $*N_2 + 6H_2O + 6e^- \rightarrow * + 2NH_3 + 6OH^-$. Formation (through electroreduction) of Fe^0 sites on Fe_2P implies structural reorganization of surfaces of the catalytic particles: Fe-P bonds are ruptured and, in addition to iron (Fe^0) atoms, phosphorous in a form of atoms, chains or cages [80] are expected to exist at the interface. It is noteworthy that, it has been recently postulated that Fe-centers within phosphorous monolayers, while interacting with P sites, can effectively activate N_2 and catalyze N_2RR [51]. Furthermore, the existence of the vacant 3*d*-orbital in Fe and the 3*p*-lone-pair electrons in P-atoms was postulated to effect charge transfer resulting in a change of the iron surface electron density which facilitates adsorption of hydrogen atoms [66,67,70,74].

For comparison, we also provide the voltammetric characteristics of FeP and Fe_3P recorded in the presence (solid lines) and absence (dashed lines) of nitrogen (Fig. 3B and 3C). As before (Fig. 3A), the voltammetric scans have been initiated (toward negative potentials) from the fairly

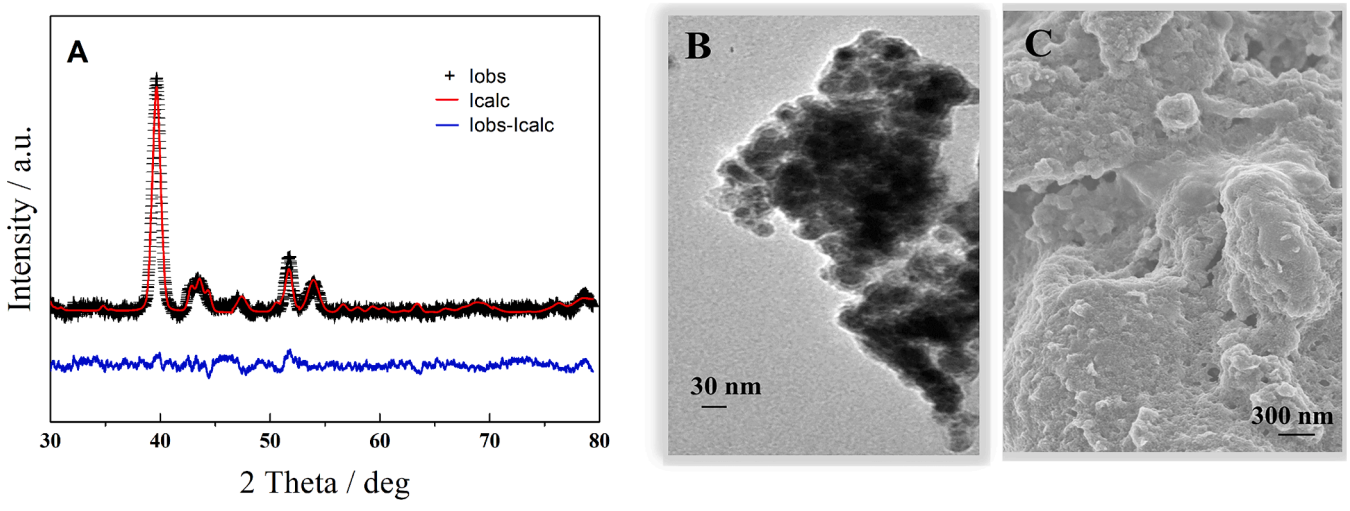

Fig. 2. (A) XRD pattern of the synthesized Fe_2P catalyst recorded upon its activation at 450°C. **(B)** Transmission electron microscopic and **(C)** scanning electron microscopic images of Fe_2P.

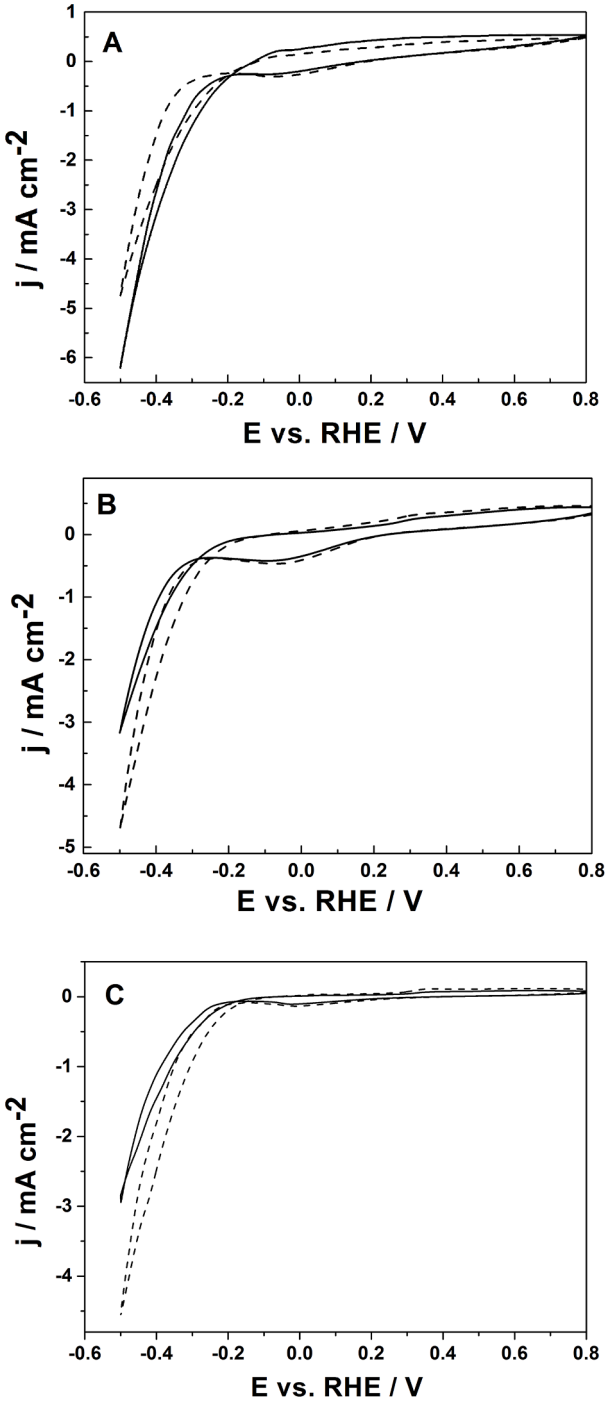

Fig. 3. Cyclic voltammetric responses recorded at 10 mV s^{-1} for (**A**) Fe_2P, (**B**) FeP, (**C**) Fe_3P films (deposited on glassy carbon) in the argon-saturated (dashed lines) and the nitrogen-saturated (solid lines) 0.5 mol dm^{-3} NaOH solutions.

positive potential of 0.8 V (vs. RHE) where surfaces of iron phosphides are partially oxidized. To avoid excessive hydrogen evolution or the compound's degradation, care has been exercised to apply neither too negative nor too positive potentials. As already mentioned, the small voltammetric peaks appearing in the range from 0.5 to 0.8 V refer most likely to iron(III)/iron(II) redox transitions at the electrocatalytic interface. Furthermore, generation of metallic iron (through electroreduction of the surface iron ions mentioned above) has tended to proceed in 0.5 mol dm^{-3} NaOH at potentials lower than -0.2 V. But upon application of potentials even lower than -0.3 V (vs. RHE), where iron has certainly existed in a form of metallic (Fe^0) sites, the hydrogen evolution reaction becomes operative. Nevertheless, contrary to the performance of Fe_2P, upon saturation the solution with nitrogen, the N_2RR currents have had tendency to decrease upon application of FeP and Fe_3P, relative to the competitive hydrogen evolution, most likely due to the appearance of inhibiting NH_3-type adsorbates. Indeed, high polarity and propensity for forming hydrogen bonds makes ammonia a sticky compound. Apparently, interfacial structures and catalytic activities of FeP and Fe_3P (in alkaline medium) are different than those of Fe_2P, and they tend to induce more effectively hydrogen evolution, rather than N_2RR. Electroreduction of nitrogen can also be operative in the cases of FeP and Fe_3P (Fig. 3B and 3C) but, here, the hydrogen evolution is not only competitive but becomes also the predominant reaction hiding the N_2 reduction. Because the passivating effects seem to be more severe and, effectively, the observed currents have tend to decrease in the hydrogen evolution region (in the presence of N_2), systematic studies of those iron phosphides have not been pursued here.

Some attention has also been paid to the catalytic properties of Fe_2P during electroreductions of such inert reactants as CO_2, O_2, and NO_2^- in alkaline medium. While the lack of any appreciable electrocatalytic properties toward CO_2-reduction is not surprising (for simplicity, the respective response is not shown here) because carbon dioxide exits (in 0.5 mol dm^{-3} NaOH) in a form of the electrochemically-highly-inert trigonal carbonates (CO_3^{2-}), the Fe^0 sites, which are postulated to exist below -0.2 V at Fe_2P, seem to catalyze effectively not only evolution of hydrogen (Fig. 4, Curve a) but electroreductions of O_2 and NO_2^- (Fig. 4, Curves b and c). The present results (Fig. 5), together with our previous data describing electrocatalytic properties of iron phosphides toward reduction of NO_3^-, imply strong reductive electrocatalytic properties of Fe^0 centers generated on Fe_2P surfaces.

3.3. *Examination of N_2RR products*

Ammonia, which is expected to be the main N_2RR product, can be identified and determined using electroanalytical methodology [72]. Despite complexity of the mechanism for oxidation of ammonia, the analytical concept refers to the previous findings describing proportionality of the electrocatalytic NH_3-oxidation currents on ammonia concentration even below mmol dm^{-3} level [81]. In the present study, N_2RR was first carried out at Fe_2P-catalyst-modified glassy carbon electrode (electrolysis for 2 h upon application of the constant potential, -0.4 V) in the nitrogen-saturated 0.5 mol dm^{-3} NaOH solution (50 dm^{-3}; N_2-concentration, 0.72 mmol dm^{-3}). At the same time, an additional Pt-based electrode was placed in the vicinity of the Fe_2P catalytic electrode. Immediately after the electrolysis step, an independent stripping-type voltammetric diagnostic experiment was performed with

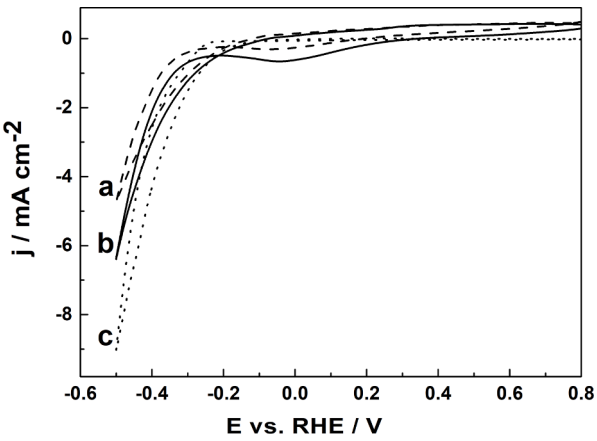

Fig. 4. Cyclic voltammetric responses recorded at 10 mV s^{-1} for Fe_2P film (deposited on glassy carbon) in 0.5 mol dm^{-3} NaOH saturated with (**a**) argon, (**b**) O_2, and (**c**) NO_2^-.

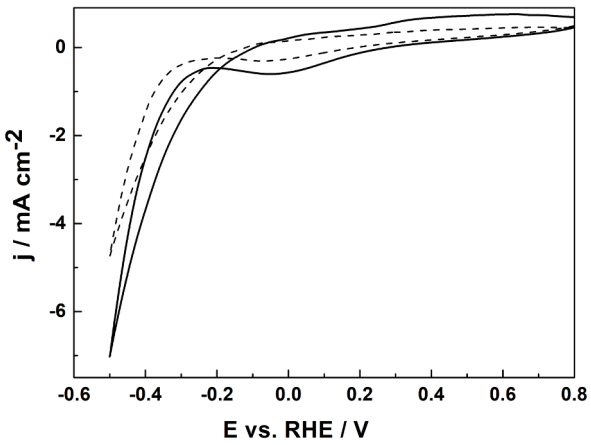

Fig. 5. Cyclic voltammetric responses recorded at 10 mV s^{-1} for Fe_2P film (deposited on glassy carbon) in 0.5 mol dm^{-3} NaOH the presence of NO_3^-.

use of an additional working electrode, in a form of Pt nanoparticles (loading 100 μg cm^{-2}) introduced onto ceria (CeO_2 nanoparticles of 30-40 nm diameters, loading, 350 μg cm^{-2}) deposited on glassy carbon electrode substrate. Here, ceria acts as support for Pt nanoparticles and facilitates their uniform distribition at the electrocatalytic interface. The actual calculations of real surface areas characteristic of Pt nanoparticles have been based on assumption that hydrogen atom can be adsorbed on a single platinum surface center where a total charge transfer occurs there [82]. Thus by integrating the areas under hydrogen adsorption peaks corrected for the background current, and by using a conversion factor of 210 μC cm^{-2}, the value of 40 m^2 g^{-1} was obtained for Pt in the presence of CeO_2.

Fig. 6 illustrates results based on a series of reference NH_3-oxidation voltammetric experiments performed in 0.5 mol dm^{-3} NaOH containing NH_3 in the concentration range from 0 to 0.20 mmol dm^{-3}. The proportionality of the oxidation peak-current densities on concentration is evident from Fig. 6A. Because, as it has recently pointed out by

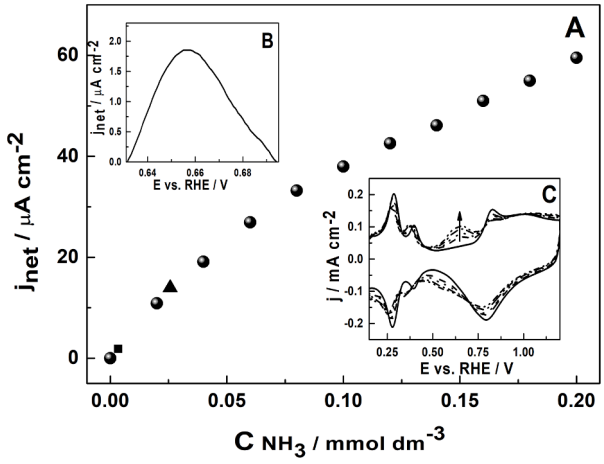

Fig. 6. Results of analytical voltammetric experiments performed at 10 mV s^{-1} using glassy carbon electrode modified with CeO_2-supported Pt nanoparticles in 0.5 mol dm^{-3} NaOH electrolyte. (**A**) Dependence of the oxidation peak current on ammonia concentration (standard solutions); (**B**) The background-subtracted voltammetric response recorded for a blank sample obtained following electrolysis for 7200 s at Fe_2P in argon-saturated electrolyte; (**C**) Cyclic voltammetric responses recorded for standard NH_3-solutions in the concentration range from 0 to 0.20 mmol dm^{-3}. Solid line stands for the response in the argon saturated (NH_3-free) solution. The triangle and square points in the working curve (Curve A) stand for the responses characteristic of the electrolyzed solutions, nitrogen-saturated and argon-saturated, respectively.

atmospheric scientists, ammonia can act as pollutant and affect urban air quality [83], we have also considered a blank experiment (Fig. 6B), namely, by performing the electrolysis step, as before, for 2 h upon application of the constant potential of -0.4 V but in the absence of nitrogen (i.e. in argon saturated solution).

In the electroanalytical approach, the voltammetric peaks, which are characteristic of ammonia oxidation, have been developed at potentials 0.55-0.75 V, and they are well-defined (Fig. 6C). The solid black line stands for the typical response of Pt nanoparticles in NH_3-free alkaline medium [81,84]. As expected, in the potential range from 0 to 0.4 V, hydrogen adsorption peaks are developed and, at potentials higher than 0.7 V, the reversible oxidation of platinum to platinum oxides becomes operative. In the middle, i.e., in the potential range from 0.4 to 0.7 V, platinum exists mostly in the metallic form. When it comes to the oxidation ammonia (Fig. 6C), it is catalyzed by metallic platinum, rather than Pt oxides, and it proceeds to nitrogen [81,84]. Platinum oxides are expected to inhibit the oxidation ammonia; on the other hand, judging from the data of Fig. 6C, formation of Pt oxides tends to be suppressed in presence of ammonia, as evident form the decreases of the oxidation currents (at potentials higher than 0.8 V) upon increasing the NH_3-concentration. The latter results are consistent with strong adsorptive interactions of ammonia with platinum, particularly Pt-oxide, surfaces in alkaline medium.

The obtained here working curve (Fig. 6A) implying proportionality of the NH_3-oxidation peak-currents on NH_3-concentration has been further used for analytical determinations. The voltammetric response (in a form a small but single peak) characteristic of the oxidation N_2RR product (which was generated at the Fe_2P catalytic electrode upon application of -0.4 V) was detected at the neighboring Pt-containing electrode (Fig. 7A). Simple comparison of the net voltammetric-peak-current density (Fig. 7B) with the data (i.e., the current-density values recorded at different concentrations (working curve in Fig. 6A), the NH_3-concentration generated following N_2RR at F_2P–modified electrode was found to be on the level 0.3 mmol dm^{-3}. When the latter value was corrected for the potential contribution originating from the atmospheric NH_3-contamination, the realistic N_2RR-product (NH_3) concentration was estimated to be equal to 0.25 mmol dm^{-3}. The blank experiment was performed in the same manner as in a case of N_2-electrolysis (electroreduction for 2 h upon application of -0.4 V, followed by the voltammetric stripping-type analytical determination of N_2RR product) but using argon-saturated solution. The experiment permitted to quantify the amount of ammonia (ca. 0.05 mmol dm^{-3}) originating

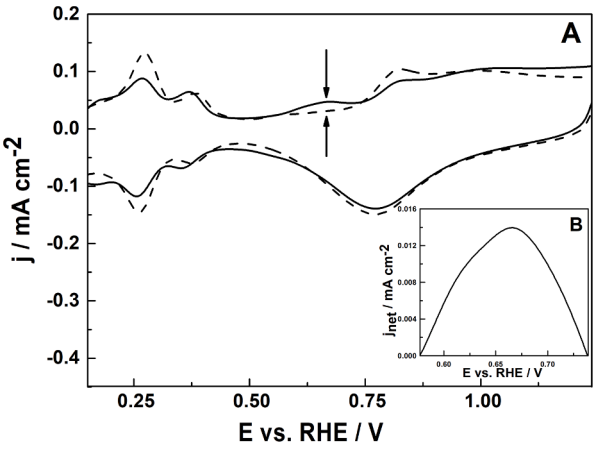

Fig. 7. (**A**) Cyclic voltammetric responses recorded (at 10 mV s^{-1}) before (dashed line) and after (solid line) N_2RR electrolysis (performed at the Fe_2P-electrode) with use of the neighboring electrode modified with CeO_2-supported Pt nanoparticles. Electrolyte: 0.5 mol dm^{-3} NaOH. (**B**) The background subtracted voltammetric oxidation current recorded at CeO_2-supported Pt nanoparticles in the solution following N_2RR electrolysis.

from potential contamination that may appear the electrolysis (e.g., due to uncontrolled leaks), electrolyte, and in such components as electrode materials.

The appearance of a single peak at about 0.65 V at Pt-based electrode (Fig. 7A and 7B) supports our view that NH_3 has been the main N_2RR product generated at the neighboring F_2P–modified electrode. In particular, no hydrazine is expected to be formed (at Fe_2P) because its oxidation would start to proceed on platinum in alkaline medium at definitely less positive potentials, namely closer to 0.25 V [85], what obviously has not been observed in Fig. 7A. It is noteworthy that the appearance of some oxidation currents at potentials higher than 0.9 V (compare solid and dashed lines in Fig. 7A) most likely reflects the Pt-oxide-induced oxidation of the reaction intermediates which are formed during oxidation of NH_3 to nitrogen-oxo-species [86]. The latter process does not seem to interfere with the analytical diagnosis because it can be easily separated from that of analytical importance, namely the voltammetric peak at about 0.65 V. The emergence of the reduction currents at about 0.2 V in the reverse voltammetric scans (Figs. 7A and 6C) should be correlated with the reduction of the surface nitrogen-oxo-species mentioned above (such as nitrates or nitrogen oxides).

To get better insight into the chemical identity of the Fe_2P-induced N_2RR product, we performed Raman measurements (Fig. 8A) to verify absence or presence of the adsorbates or deposits of ammonia molecules on Pt nanoparticles (on the neighbouring electrode) depending whether the electrolysis was performed in (a) argon or (b) nitrogen saturated electrolytes. In this diagnostic experiment, platinum was deposited directly onto glassy carbon, i.e., without ceria (CeO_2) underlayer to avoid complications in the interpretation of Raman spectra. For clarity of presentation, the obtained Raman spectra were raised up in the region from 1200 to 1750 cm^{-1}, where differences in the Raman responses (Curves a and b) were evident (Fig. 8B). The appearance of strong signals in all measured Raman spectra, the vibrations at 3270 cm^{-1} and 3440 cm^{-1} should be correlated to the OH-group stretching vibrations, symmetrical and asymmetrical, respectively [87,88]. The H-O-H bending bands existing at about 1621 cm^{-1} were generally much less visible. In a case of the spectrum characteristic of the electrode taken out from the solution where the electrolysis had been performed in the presence of argon (N_2-free solution), only the bands originating from water molecules were visible (Fig. 8A, Curve a). Additional bands appeared following the electrolysis involving nitrogen (Fig. 8A, Curve b). The peaks emerging at frequencies of 1361 and 1564 cm^{-1} could be assigned to ammonium deformation (Fig. 8B, Curve b) [89,90]. Unfortunately, the main band characteristic of ammonium molecule at about 3300 cm^{-1} (corresponding to the symmetrical stretching vibrations of the N-H bond) was damped by quite a large signal from water (Fig. 8A). Although, the regions between 1550-1610 cm^{-1}, 1320 -1370 cm^{-1}, and the peak appearing at around 2691 cm^{-1} are often attributed to G, D, and to the overtone of the D mode (so-called 2D peak) of amorphous carbon [91], their existence at our platinized electrode substrates was unlikely. Indeed, the G and D signals mentioned above were almost completely absent for the sample obtained following electrolysis in the N_2-free solution (Fig. 8, Curve a). On the whole, the Raman data are consistent with the formation of ammonia during electrolysis at -0.4 V in the nitrogen-saturated NaOH electrolyte.

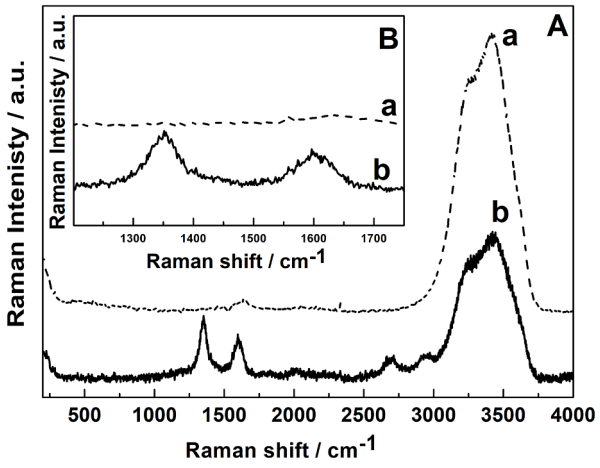

Fig. 8. Raman spectroscopic measurements performed for deposits at platinized glassy carbon electrode following electrolysis at Fe_2P electrode in (**a**) argon-saturated and (**b**) nitrogen-saturated 0.5 mol dm^{-3} NaOH solutions. The spectra are presented in the following regions: (**A**) from 700 to 4000 cm^{-1}, and (**B**) from 1200 to 1750 cm^{-1}.

3.4. *Efficiency, durability and dynamics of N_2RR*

Fig. 9 illustrates current-potential (chronoamperometric) responses of Fe_2P recorded upon application of the constant potential of -0.4 V (a) in the absence of nitrogen (i.e. in argon- saturated solution) and (b) in the nitrogen-saturated solution. In other words, while Curve a stands for the system's performance toward hydrogen evolution, Curve b yields the current response comprising both hydrogen evolution and N_2RR. Relative to the analogous behavior under voltammetric conditions (Fig. 3A), the selectivity of Fe_2P toward N_2RR, relative to H_2-evolution, seems to be more pronounced in chronoamperometry (Fig. 9). It is likely that, contrary to cyclic voltammetry, which involves the Fe-catalyst's re-oxidation step and possibly some reorganization, in chronoamperometry upon application of the constant potential of -0.4 V, the iron catalytic sites are continuously kept in the reduced state and, thus, they are pre-conditioned and stabilized. The long-term stability and persistence of the electrocatalytic activity of the partially reduced Fe_2P during N_2RR is evident from the steady-state character of chronoamperometric response recorded in the presence of nitrogen (Fig. 9, curve b). Furthermore, this well-behaved result excludes the existence of substantial inhibiting or poisoning effects. Some current distortions observed during chronoamperometric N_2RR (Curve b), including that at $t > 6000$, do not have reproducible character, and they may reflect local structural reorganizations which do not lead to the observable degradation or deactivation of the catalyst. It is likely that the theoretically postulated interactions between the iron catalytic centers and phosphorous sites [51] not only activate the N_2 inert molecule but also diminish a possibility of the far-reaching passivation of the catalyst, e.g. by accumulation of NH_3 (reaction product) at the interface. While the presence of Fe and P could be confirmed on the catalytic surfaces, we were unable using Raman spectroscopy to comment about the chemical identities and oxidation states of Fe and P neither before nor after the

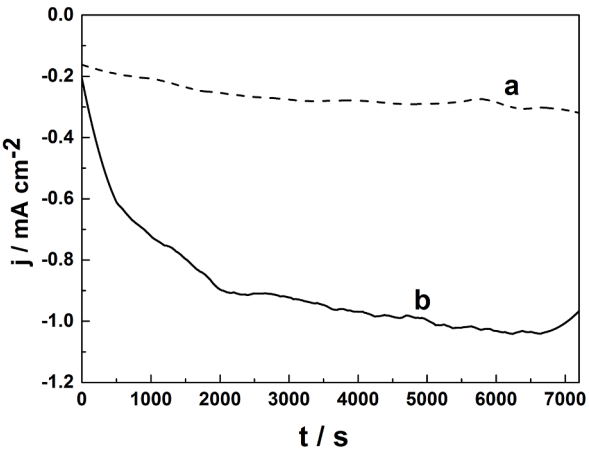

Fig. 9. Chronoamperometric responses recorded at Fe_2P upon application of the constant potential of -0.4 V (**a**) in the absence of nitrogen (i.e. in argon-saturated solution), and (**b**) in the nitrogen-saturated solution.

electrocatalytic measurements.

The estimation of Faradaic effciency for ammonia formation has been based on the assumption that ammonia is the only N-containing reaction product, as well as that the generation of NH_3 (1 mole) is the three-electron process ($^1/_2N_2 + 3H_2O + 3e^- \rightarrow NH_3 + 3OH^-$), and formation of the competitive H_2 (1 mole) is the two-electron reaction ($2H_2O + 2e^- \rightarrow H_2 + 2OH^-$). Based on supposition that the contribution from hydrogen evolution is approximately on the same level in the presence and absence of nitrogen, first, we have referred the chronoamperometric data of Fig. 9 and considered values of the representative steady-state currents recorded after sufficiently long time, 6500 s, in (**a**) absence and (**b**) presence of nitrogen. To compare the respective current values, the value characteristic of the current recorded in the presence of nitrogen (1.03 mA cm^{-2}) has been corrected for the contribution originating from the hydrogen evolution (0.30 mA cm^{-2}) to yield the net-current value, 0.73 mA cm^{-2}. By comparing the respective current densities, it can be rationalized that ca. 70% of the flowing current stands for NH_3-formation. Remembering that different numbers of electrons are involved in both processes, the selectivity (molar) efficiency can be estimated to be on the level 62%. Furthermore, by taking into account the amount of charge (0.46 C) transferred after the electrolysis for 7200 s at the Fe_2P-electrode (Fig. S1), correcting it for the contribution originating from hydrogen evolution (0.14 C), we have obtained the net-charge assigned to NH_3-formation, 0.32 C. The latter value can be recalculated to the ammount of the generated product, $1.1*10^{-6}$ mol of NH_3. Based on the independently determined concentration of ammonia, 0.025 mmol dm^{-3}, following electrolysis in 40 cm^{-3} of NaOH electrolyte, the ammount of the generated NH_3 was found to be equal to ca. $1.0*10^{-6}$ mol of NH_3. The obtained values, $1.1*10^{-6}$ mol and $1.0*10^{-6}$ mol are almost identical despite uncertainty in analytical determination or in the assumption about the hydrogen evolution dynamics in the presence of ammonia. On the whole, it can be stated that the Faradaic efficiency, which in a sense is the selectivity (molar) efficiency, toward production of NH_3 is on the level of 60%.

Furthermore, the yield rate has been estimated during N_2RR electrolysis at -0.4 V for 7200 s performed at Fe_2P-modified electrode and found to be equal to 7.5 μmol cm^{-2} h^{-1} (21 μmol m^{-2} s^{-1}). Of course, due to some uncertainty in determination and identification of NH_3 as the N_2-reaction product, the above parameters are obviously estimates. If we consider the loading of Fe_2P catalyst (4.9 mg cm^{-2}), the NH_3-yield would reach the value of 26 μg h^{-1} mg^{-1}. It should be remembered that, in the latter case, the only small (surface) fraction of Fe_2P is electroactive, so the yield expressed per mg of Fe_2P could be somewhat underestimated. Comparison to the existing literature [2,3,8,11,12,16,18,22] is not straightforward because the analogous parameters were measured in different electrolytes and upon application of distinct potentials. Nevertheless, having in mind the activity of the iron-group electrocatalysts for N_2RR at ambient conditions [40], the values here are not only competitive, but they are also consistent with the reasonably high electrocatalytic activity of Fe_2P during N_2RR (upon application of -0.4 V vs RHE) in alkaline medium.

Some attention has also been paid to the performance of Fe_2P-modified electrode during the N_2RR electrolysis (for 7200 s; as for Figs. 9 and S1) but at different potentials, -0.5 and -0.3 V. As in a case of the measurement at -0.4 V, by considering the amounts of charge transferred after the electrolysis (corrected for the contributions originating from hydrogen evolution), the following yield rates, 6.9 μmol cm^{-2} h^{-1} (20 μmol m^{-2} s^{-1}) and 3.5 μmol cm^{-2} h^{-1} (10 μmol m^{-2} s^{-1}) upon application of the more negative, -0.5 V, and less negative, -0.3 V, potentials. Thus the Fe_2P catalyst has exhibited the highest yield rate (7.5 μmol cm^{-2} h^{-1} or 21 μmol m^{-2} s^{-1}) for ammonia generation at -0.4 V (vs. RHE). Application of more negative potential (-0.5 V) leads to comparable result (rather than to the efficiency increase), mainly due to competitive hydrogen evolution that seems to be more excessive under conditions of prolonged electrolysis, relative to the voltammetric reduction. As expected, the yield rate significantly decreases at less negative potential of -0.3 V, most likely as a consequence of kinetic limitations.

3.5. Mechanistic considerations

Both hydrogen evolution and nitrogen reduction are proton-coupled electron-transfer reactions. In the latter case, a sequence of multiple steps is required for the complete conversion of nitrogen to ammonia. It is reasonable to expect that the competing two-electron hydrogen evolution is likely to be kinetically preferred over the more complex multistep six-electron nitrogen reduction. The so called Butler−Volmer model and the current−potential relationships and related equations, illustrated in a form of Tafel plots have been widely used to elucidate electrocatalytic mechanisms and to provide valuable kinetic information [92]. Although the exact value of Tafel slope characteristic of a specific electrocatalytic N_2RR process has not as yet been clearly determined, depending on the actual importance N_2-activation and proton transfer, i.e., of whether the first electron transfer, or the first proton transfer, is the rate-limiting step in the electrocatalytic N_2RR process, the Tafel slope of N_2RR current densities could be 60 mV per decade (mV/dec), 120 mV/dec, or larger than 120 mV/dec [93,94].

Fig. 10 shows the Tafel relationships, namely potential versus log|*i*| (logarithm of current density) for N_2RR at Fe_2P recorded in N_2-aturated 0.5 mol dm^{-3} NaOH. There are two distinctive regions in the Tafel plot characterized by different slopes, ca. 37 mV dec^{-1} and 350 mV/dec. This result is consistent with the view that the rate determining steps in the N_2RR mechanism change depending on the applied potential. The small Tafel slope (~37 mV/dec), which is observed initially (Fig. 10, line a), i.e., in the potential range 0.25-0.30 V, may imply faster kinetics or better catalytic activity at lower overpotentials where the competing hydrogen evolution is not so advanced. But the much larger slope (~350 mV dec^{-1}) observed at potentials exceeding 0.35 V (Fig. 10, line b) may reflect some decrease of activity at larger overpotentials due to the catalyst partial deactivation, e.g., through poisoning with NH_3-product or existence of competitive hydrogen evolution. It is difficult to postulate degradation of the catalyst under such conditions because its preconditioning at -0.4 or -0.5 V tends to increase its activity. The high Tafel slope values in 0.5 mol dm^{-3} NaOH may suggest that limitations in proton availability and transfer, or discharge, could be the rate-determining step on the surface of a catalyst [95]. Remembering that both hydrogen evolution and N_2RR appear in the same potential range, it is likely that hydrogenation of the adsorptively-activated N_2-molecule involving a series of hydrogen and electron transfers is triggered by the reductive water splitting.

It was also apparent from impedance measurements that relative

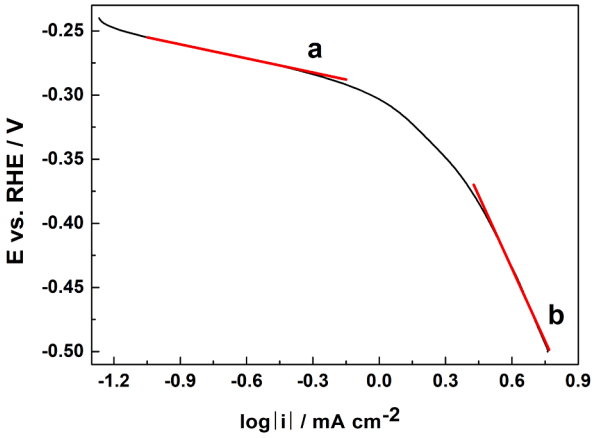

Fig. 10. Tafel relationship for N_2RR at Fe_2P plotted on the basis of voltammetric data (background subtracted currents recorded in N_2-aturated 0.5 mol dm^{-3} NaOH) of Fig. 3A.

significance of hydrogen evolution and nitrogen reduction highly depended on electrode potential. Electrochemical impedance spectroscopy (EIS) was employed to comment on the charge transfer resistance (R_{ct}) at the surface of electrocatalysts in 0.5 mol dm^{-3} NaOH in argon (N_2-free) and nitrogen saturated solutions [96]. Nyquist plots, which represent negative of the imaginary versus the real parts of the complex impedance characteristic of the Fe_2P film, were recorded upon application of potentials ranging from -0.1 to -0.4 V vs. RHE (Fig. 11). The characteristic semicircle type responses started to appear at -0.2 V or lower potentials where both hydrogen evolution and nitrogen reduction were operative. Shapes of semicircles were somewhat different in the presence and absence of nitrogen: two impedance loops (high and low frequency) were observed in N_2 due to the fact that both N_2RR and hydrogen evolution were operative, whereas one loop appeared in Ar where only hydrogen evolution was in force. The charge transfer resistances are generally comparable in Ar and N_2 saturated solutions. However, a slight increase in the Faradaic impedance in N_2-solution (relative to Ar-solution) observed at -0.4 V may suggest that N_2RR was somewhat more sluggish in the presence of nitrogen and could slow down hydrogen evolution. On the other hand, the charge transfer resistance seemed to be somewhat lower at -0.2 V in presence of nitrogen, in comparison to N_2-free solution, because the reaction mechanism was apparently different upon application of the less negative potential. On the whole, the impedance data indicate that both nitrogen reduction and hydrogen evolution reactions occurred in parallel, and charge transfers were determined by both processes no matter which one was dominating or relatively more efficient.

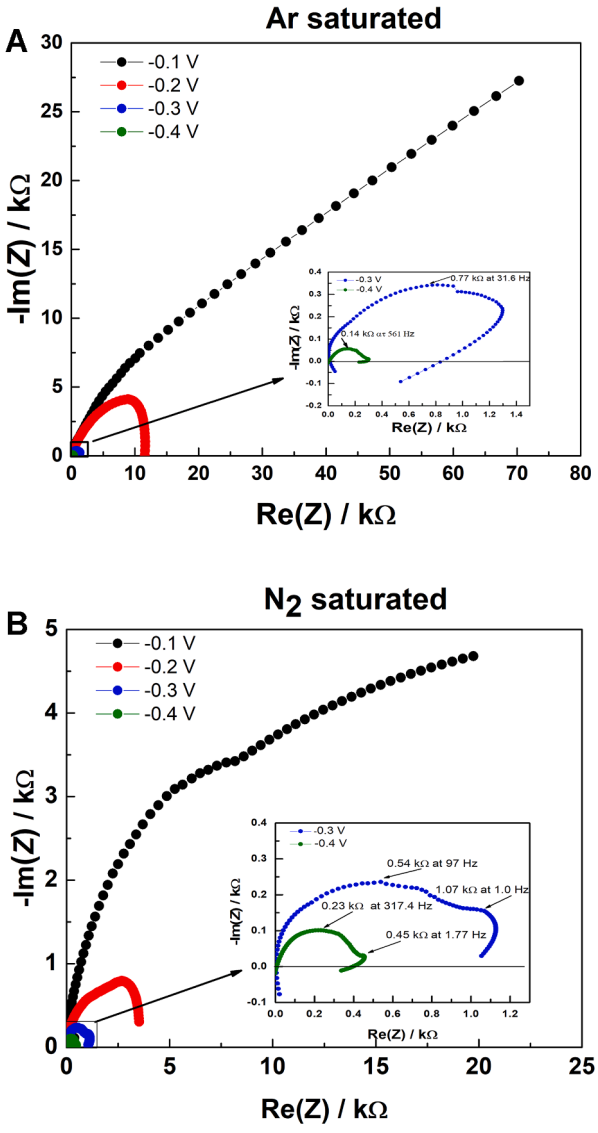

Fig. 11. Nyquist plots (which represent negative of the imaginary versus the real parts of the complex impedance) recorded for Fe_2P in (A) argon and (B) nitrogen saturated solutions upon application of potentials ranging from -0.1 to -0.4 V (vs. RHE).

Based on above observations, it is reasonable to expect that N_2RR at Fe_2P is controlled by kinetics of electron transfer, rather than by mass transport in solution. Indeed, when the experiment of Fig. 3A has been repeated at scan rates in the range 5–50 mV s^{-1}, the observed N_2RR voltammetric currents (e.g., measured at -0.4 V) have barely increased with growing can rate. Also the respective net, background (i.e., measured in argon) subtracted, voltammetric currents have been largely independent of scan rate. Thus, it can be assumed that the present electrocatalytic system is kinetically slow enough to be considered as totally dependent on interfacial charge transfer rates rather than diffusional mass transport. Then the classic kinetic equation is applicable here [92,97,98]:

$$j = nFk_bC^* \quad (3)$$

where j refers to current density of the background-subtracted steady-state chronoamperometric response (in A cm^{-2}) obtained from Fig. 9, e.g., after 4000 s during electrolysis at -0.4 V; n is a number electrons involved (here n = 6), F is Faraday constant (96500 C mol^{-1}), k_b is the rate constant for N_2RR in heterogeneous units (cm s^{-1}), and C^* stands for bulk (solution) concentration (N_2-concentration, 0.72 mmol dm^{-3} in nitrogen-saturated 0.5 mol dm^{-3} NaOH). The obtained k_b value is on the level 1-2*10^{-4} cm s^{-1}. Because the actual contribution from hydrogen evolution and a value of the net N_2RR current are uncertain, the present result is approximate. Nevertheless, using the heterogeneous rate constant units (in cm s^{-1}), which are commonly used in electrochemistry to judge about rates of electron transfers, the Fe_2P system's activity toward N_2RR in alkaline medium can be viewed as kinetically moderate. When compared to the slow irreversible systems characterized by k_b's on the level of 10^{-6} cm s^{-1} or lower, the present rate constant on the level of 10^{-4} cm s^{-1} is more than two orders of magnitude higher. On the other hand, when compared to the dynamics of oxygen reduction at Pt electrodes in acid medium [98], the present value is ca. two orders of magnitude lower.

3.6. Validation of measurements

Our attention has also centered on verification of the quality of nitrogen in the feed stream. In this respect, a series of diagnostic voltammetric experiments have been performed using the catalytic systems exhibiting highly specific electroreduction activities toward potential contaminants, such as traces of oxygen or nitrogen oxides. The actual diagnostic experiments have involved N_2-bubbling for 2 h with no applied potential (i.e., under open circuit conditions). Here Pt nanoparticles, which are broadly studied in fuel cell research [99–101], have been utilized to induce electrochemical reactions of potential contaminants (oxygen, nitrogen oxide species etc.). First, we have performed a diagnostic experiment by recording comparative cyclic voltammograms characteristic of Pt nanoparticles in Ar-bubbled (solid line) and in N_2-bubbled (dashed line) alkaline (0.5 mol dm^{-3} NaOH) solution (Fig. 12). The responses are typical for the interfacial behavior of Pt in alkaline medium [84], and they are practically indistinguishable in the presence of nitrogen and argon. In both cases, the identical hydrogen adsorption peaks are developed in the potential range from 0 to 0.4 V, and, at potentials higher than 0.7 V, exactly the same patterns for the reversible oxidation of platinum to platinum oxides have been observed. In between hydrogen peaks and formation of Pt oxides, platinum exists mostly in the metallic form. All these three regions (potential-dependent Pt-surface chemical identities) exhibit various electrocatalytic

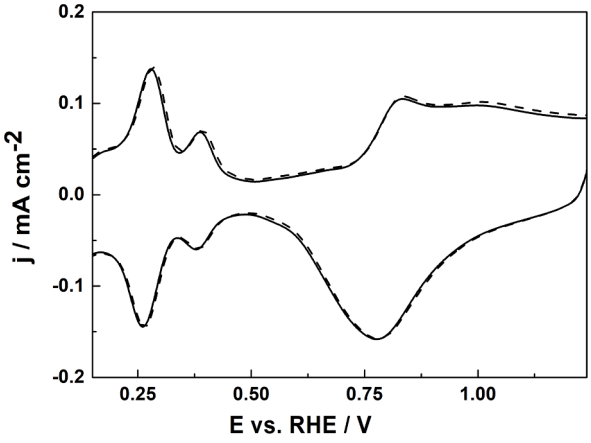

Fig. 12. Cyclic voltammograms characteristic of Pt nanoparticles in Ar-bubbled (solid line) and in N_2-bubbled (dashed line) alkaline (0.5 mol dm^{-3} NaOH) solution. Scan rate, 10 mV s^{-1}.

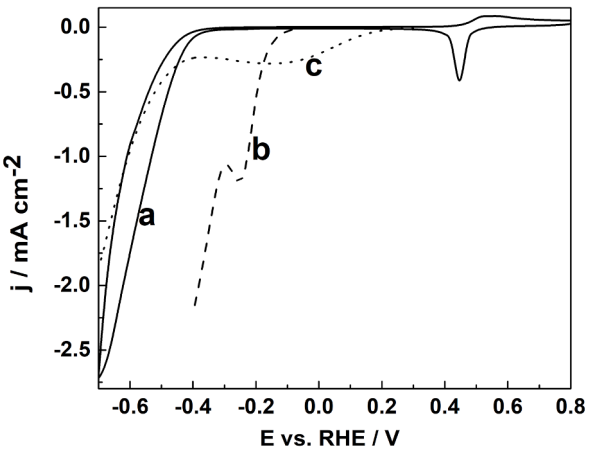

Fig. 13. Voltammetric behavior of the glassy carbon electrode modified with HKUST-1 in deoxygenated (Ar-saturated) phosphate buffer solutions (Curves a and b) in the absence (a) and in the presence (b) of nitrates (NO_3^-). Curve c stands for the response in presence of oxygen. Scan rate, 10 mV s^{-1}.

properties [99–101], e.g., toward reduction of nitrogen oxides (H-adsorption sites), reduction of oxygen (Pt^0 sites), or oxidation of small organic molecules (Pt-oxide). The cyclic voltammograms of Fig. 12 have been recorded in the enough broad range of potentials to induce the redox reaction mentioned above, if the respective impurities exit in the solution. The identical responses obtained for the inert argon and the investigated nitrogen Fig. 12 imply the absence of any additional redox processes originating from potential impurities in the N_2-gas.

Effectiveness of the electrocatalytic reductions of oxygen and nitrogen oxides are the most pronounced in acid (0.5 mol dm^{-3} H_2SO_4) medium. The appearance of any reduction voltammetric currents higher than those characteristic of the behavior of Pt nanoparticles in deoxygenated H_2SO_4 electrolyte (dashed lines in Figs. S2 and S3) [99–101] would be indicative of the existence of potential contaminants. The results of the reference experiments performed in the solutions containing oxygen (O_2) or nitrites coexisting in acid medium with nitrogen oxides, NO_x, are shown in Supplementary Information section (Figs. S2 and S3). If any O_2 or NO_x were present in the solution following N_2-bubbling for 2 h, the additional electroreduction current would appear around 0.75-0.8 V (O_2-reduction) or 0-0.3 V (NO_x-reduction), respectively. All diagnostic experiments have been repeated at least eight times in the presence of nitrogen and argon, and the recorded cyclic voltammograms have been practically identical (Fig. S4), i.e., no electrocatalytic currents from additional species (potential contaminants) have been observed. In other words, in the investigated N_2-bubbled solutions, no detectable electrocatalytic currents have been observed at Pt electrodes that could be attributed to traces of oxygen or NO_x/nitrites.

Relative to nitrites (NO_2^-) or NO_x, Pt is a less specific catalyst for reduction of nitrates (NO_3^-). Although the presence of nitrates(V) or nitrogen(V) oxides as possible contaminant is not very likely, we have considered here and additional catalytic system, a typical porous metal organic framework (MOF) material, HKUST-1 (Cu-BTC, where BTC stands for benzene-1,3,5-tricarboxylate). Here the copper active sites are coordinated by BTC linkers within octahedral cages with large cavities, and being largely unsaturated they can act as strong adsorption sites of importance to separation science and catalysis, including electrocatalysis [102–104] of importance to catalysis. More details about the HKUST-1 system used here are provided in Supplementary Information (including Fig. S5). Fig. 13 illustrates the voltammetric behavior of the glassy carbon electrode modified with HKUST-1 in deoxygenated (Ar-saturated) phosphate buffer solutions (Curves a and b) in the absence (a) and in the presence (b) of nitrates (NO_3^-). It is evident that the electrocatalytic system induces readily the reduction of nitrates at potentials much more positive (starting from ca. -0.1 V), in comparison to hydrogen evolution (starting from ca. -0.4 V). It is also noteworthy that nitrites (NO_2^-) are also reduced at the same potentials (for simplicity the result is not shown here). For comparison, the system's response in the presence of oxygen (Curve c) is also provided: the reduction of oxygen starts at the potential as positive as ca. 0.2 V. Finally, it should mentioned that Curve a, which stands in Fig. 13 for the behavior of HKUST-1 in the deoxygenated (Ar-saturated) electrolyte, is exactly reproduced when the experiment is repeated under analogous conditions except that the electrolyte has been saturated with nitrogen. The results of Fig. 13 are consistent with the view that (*i*) nitrogen is not electroactive (i.e., it does not undergo reduction) in the investigated range of potentials, and (*ii*) no responses that can attributed to the reduction of nitrates or oxygen have been detected in N_2-bubbled solutions. Once more, we have no evidence for the existence of nitrogen oxo-species in the N_2-gas. Finally, on mechanistic grounds, while the set of small surface peaks at about 0.4-0.5 V shall be attributed to the fairly reversible Cu^{II}/Cu^{I} redox transition, as well as hydrogen evolution (below -0.4 V) shall be correlated with the formation of Cu^0 species, it is reasonable to expect that the electrocatalytic reductions of oxygen and nitrates proceed at BTC-coordinated active Cu^{I} sites upon application of sufficiently negative potentials. The topic will be a subject of separate publication but, at present, the HKUST-1 based system has been considered as sensing material for electrocatalytic probing of potential contaminants.

In principle, the proposed electroanalytical approach, which is performed in a sealed system (without opening of electrochemical cell), permits reliable determination of ammonia. Special attention should be paid to the proper insulation of the electrochemical cell from air during electrolysis (N_2RR) followed by the voltammetric determination at the neighboring platinized electrode. Any exposure to air (e.g., through leaks) would result in contamination not only with oxygen but also with traces of ammonia that exist at ambient conditions [105].

The concentration of the resulting NH_3 was also measured using the indophenol blue method by recording the spectrum in the visible range from 575 to 725 nm. Preparation of solutions for determinations was done as described elsewhere [106]. The indophenol blue formed was determined by absorbance at the wavelength of 650 nm. While Fig. S6A illustrates the results for the reaction product obtained after N_2RR electrolysis for 2 h at -0.4 V (upper red spectrum) and for the blank (background) experiment performed under analogous conditions but in the presence of argon (lower black spectrum), Fig. S6B shows the result for a representative standard solution of a known concentration, 0.06 mmol dm^{-3} NH_3. Simple comparison of spectra in Fig. S6, as well as consideration of a standard curve (absorbance = 0.130 C_x + 0.000210; where C_x stands for NH_3-concentration) showing linear regression with

R^2 value of 0.9986, implied that, although the background-corrected value of the NH_3-concentration determined as N_2RR product, 0.022 mmol dm^{-3}, was comparable to that found electrochemically (0.025 mmol dm^{-3}), the spectrophotometric method produced much higher background response probably due more frequent exposure of the investigated samples to air which was likely to contain NH_3 as contaminant. Thus special attention should be paid to performing blank measurements to control the degrees of contamination, possible uncertainty and reliability of analytical determinations.

4. Conclusions

Based on the electrochemical diagnostic experiments (cyclic voltammetry, long-term electrolysis, chronoamperometry), evidence is provided for the remarkable catalytic activity of Fe_2P toward electroreduction of N_2 in alkaline medium. The system's activity shall be attributed to the formation of Fe^0 catalytic centers, coexisting and most likely interacting with P sites, on surfaces of Fe_2P nanoparticles or their agglomerates. The results of both Raman spectroscopic, spectrophotometric and voltammetric stripping-type (at Pt-based electrode) measurements imply that, in addition to the evolution of hydrogen, NH_3 is the main reaction product. Based on electrocatalytic diagnostic experiments (utilizing Pt nanoparticles and HKUST-1) care has been exercised to control purity of nitrogen gas and to probe presence of potential contaminants such as ammonia, nitrogen oxo-species and oxygen. The results of impedance measurements and Tafel plot analysis imply that the dynamics of N_2RR (competing with hydrogen evolution) depends on the applied potential. Based on the classic approach to kinetic electroanalysis, the rate constant in heterogeneous units has been found to be on the moderate level of $1\text{-}2*10^{-4}$ cm s^{-1} (at -0.4 V). Although the fabrication and utilization of Fe_2P has not been optimized yet, the reasonably high Faradaic efficiencies and NH_3-yields have been obtained.

CRediT authorship contribution statement

Beata Rytelewska: Investigation, Data curation. **Anna Chmielnicka:** Investigation, Data curation. **Takwa Chouki:** Investigation, Resources. **Magdalena Skunik-Nuckowka:** Validation, Resources. **Shaghayegh Naghdi:** Validation, Resources. **Dominik Eder:** Validation, Resources, Supervision. **Aleksandra Michalowska:** Validation, Resources. **Tomasz Ratajczyk:** Resources. **Egon Pavlica:** Resources. **Saim Emin:** Validation, Resources, Supervision. **Yongsheng Fu:** Validation, Resources. **Iwona A. Rutkowska:** Conceptualization, Supervision, Methodology, Investigation, Data curation, Formal analysis, Writing – original draft, Writing – review & editing. **Pawel J. Kulesza:** Conceptualization, Methodology, Supervision, Formal analysis, Writing – original draft, Writing – review & editing.

Declaration of Competing Interest

The authors declare that they have no known competing financial interests or personal relationships that could have appeared to influence the work reported in this paper.

Data availability

Data will be made available on request.

Acknowledgments

This work was financially supported by the National Science Center (NCN, Poland) initially under the grant Opus Project 2018/29/B/ST5/02627 and, later, under Opus Lap Project 2020/39/I/ST5/03385. This work was also supported by the Austrian Science Fund (FWF,I 5413-N) and Slovenian Research Agency under the trilateral project (N2-0221) for scientific cooperation between the Republic of Slovenia, the Republic of Austria, and the Republic of Poland. Anna Chmielnicka was supported in part by University of Warsaw under IDUB framework IV.4.1. A complex programme of support for UW PhD students –microgrants, 2nd edition (BOB-IDUB-622-404/2022). S. Emin and T. Chouki acknowledge the financial support from the Slovenian Research Agency (research core funding: P2-0412).

Supplementary materials

Supplementary material associated with this article can be found, in the online version, at doi:10.1016/j.electacta.2023.143360.

References

[1] S.L. Foster, S.I.P. Bakovic, R.D. Duda, S. Maheshwari, R.D. Milton, S.D. Minteer, M.J. Janik, J.N. Renner, L.F. Greenlee, Catalysts for nitrogen reduction to ammonia, Nat. Catal. 1 (2018) 490–500.
[2] C. Tang, S.Z. Qiao, How to explore ambient electrocatalytic nitrogen reduction reliably and insightfully, Chem. Soc. Rev. 48 (2019) 3166–3180.
[3] Y. Ren, C. Yu, X. Tan, H. Huang, Q. Wei, J. Qiu, Strategies to suppress hydrogen evolution for highly selective electrocatalytic nitrogen reduction: challenges and perspectives, Energy Environ. Sci. 14 (2021) 1176–1193.
[4] J.W. Erisman, M.A. Sutton, J. Galloway, Z. Klimont, W. Winiwarter, How a century of ammonia synthesis changed the world, Nat. Geosci. 1 (2008) 636–639.
[5] D.R. Kanter, F. Bartolini, S. Kugelberg, A. Leip, O. Oenema, A. Uwizeye, Nitrogen pollution policy beyond the farm, Nat. Food 1 (2020) 27–32.
[6] J.G. Chen, R.M. Crooks, L.C. Seefeldt, K.L. Bren, R.M. Bullock, M.Y. Darensbourg, P.L. Holland, B. Hoffman, M.J. Janik, A.K. Jones, M.G. Kanatzidis, P. King, K. M. Lancaster, S.V. Lymar, P. Pfromm, W.F. Schneider, R.R. Schrock, Beyond fossil fuel-driven nitrogen transformations, Science 360 (2018) 6391.
[7] S.L. Foster, S.I.P. Bakovic, R.D. Duda, S. Maheshwari, R.D. Milton, S.D. Minteer, M.J. Janik, J.N. Renner, L.F. Greenlee, Catalysts for nitrogen reduction to ammonia, Nat. Catal. 1 (2018) 490–500.
[8] H. Xu, K. Ithisuphalap, Y. Li, S. Mukherjee, J. Lattimer, G. Soloveichik, G. Wu, Electrochemical ammonia synthesis through N_2 and H_2O under ambient conditions: theory, practices, and challenges for catalysts and electrolytes, Nano Energy 69 (2020), 104469.
[9] A.J. Martín, T. Shinagawa, J. Pérez-Ramírez, Electrocatalytic reduction of nitrogen: from haber-bosch to ammonia artificial leaf, Chem 5 (2019) 263–283.
[10] X. Lv, L. Kou, T. Frauenheim, Hydroxyl-boosted nitrogen reduction reaction: the essential role of surface hydrogen in functionalized Mxenes, ACS Appl. Mater. Interfaces 13 (2021) 14283–14290.
[11] H. Tanaka, Y. Nishibayashi, K. Yoshizawa, Interplay between theory and experiment for ammonia synthesis catalyzed by transition metal complexes, Acc. Chem. Res. 49 (2016) 987–995.
[12] M.M. Shi, D. Bao, B.R. Wulan, Y.H. Li, Y.F. Zhang, J.M. Yan, Q. Jiang, Au subnanoclusters on TiO_2 toward highly efficient and selective electrocatalyst for N_2 conversion to NH_3 at ambient conditions, Adv. Mater. 29 (2017), 1606550.
[13] J.P. Mills, C. Du, Z. Chen, T. Guo, Y.A. Wu, Catalyst design strategies for aqueous N_2 electroreduction, Appl. Mater. Today 25 (2021), 101184.
[14] H.P. Jia, E.A. Quadrelli, Mechanistic aspects of dinitrogen cleavage and hydrogenation to produce ammonia in catalysis and organometallic chemistry: relevance of metal hydride bonds and dihydrogen, Chem. Soc. Rev. 43 (2014) 547–564.
[15] P. Yang, H. Guo, F. Zhang, Y. Zhou, X. Niu, *In-situ* characterization technique in electrocatalytic nitrogen reduction to ammonia, Chin. Sci. Bull. 67 (2022) 2921–2936.
[16] X. Guo, J. Gu, S. Lin, S. Zhang, Z. Chen, S. Huang, Tackling the activity and selectivity challenges of electrocatalysts toward the nitrogen reduction reaction via atomically dispersed biatom catalysts, J. Am. Chem. Soc. 142 (2020) 5709–5721.
[17] L. Li, Q. Shao, X. Huang, Amorphous oxide nanostructures for advanced electrocatalysis, Chem. Eur. J. 26 (2020) 3943–3960.
[18] R.B. Zhao, C.W. Liu, X.X. Zhang, X.J. Zhu, P.P. Wei, L. Ji, Y.B. Guo, S.Y. Gao, Y. L. Luo, Z.M. Wang, X. Sun, An ultrasmall Ru_2P nanoparticles-reduced graphene oxide hybrid: an efficient electrocatalyst for NH_3 synthesis under ambient conditions, J. Mater. Chem. A 8 (2020) 77–81.
[19] G.R. Deng, T. Wang, A.A. Alshehri, K.A. Alzahrani, Y. Wang, H.J. Ye, Y.L. Luo, X. P. Sun, Improving the electrocatalytic N_2 reduction activity of Pd nanoparticles through surface modification, J. Mater. Chem. A 7 (2019) 21674–21677.
[20] D. Bao, Q. Zhang, F.L. Meng, H.X. Zhong, M.M. Shi, Y. Zhang, J.M. Yan, Q. Jiang, X.B. Zhang, Electrochemical reduction of N_2 under ambient conditions for artificial N_2 fixation and renewable energy storage using N_2/NH_3 cycle, Adv. Mater. 29 (2017), 1604799.
[21] H.M. Liu, S.H. Han, Y. Zhao, Y.Y. Zhu, X.L. Tian, J.H. Zeng, J.X. Jiang, B.Y. Xia, Y. Chen, Surfactant-free atomically ultrathin rhodium nanosheet nanoassemblies for efficient nitrogen electroreduction, J. Mater. Chem. A 6 (2018) 3211–3217.
[22] W. Xiong, X. Cheng, T. Wang, Y.S. Luo, J. Feng, S.Y. Lu, A.M. Asiri, W. Li, Z. J. Jiang, X.P. Sun, Co_3(hexahydroxytriphenylene)$_2$: a conductive metal-organic

framework for ambient electrocatalytic N_2 reduction to NH_3, Nano Res. 13 (2020) 1008–1012.
[23] Y. Wang, M.M. Shi, D. Bao, F.L. Meng, Q. Zhang, Y.T. Zhou, K.H. Liu, Y. Zhang, J. Z. Wang, Z.W. Chen, D. Liu, Z. Jiang, M. Luo, L. Gu, Q.H. Z, X. Cao, Y. Yao, M. Shao, Y. Zhang, X.B. Zhang, J.G. Chen, J. Yan, Q. Jiang, Generating defect-rich bismuth for enhancing the rate of nitrogen electroreduction to ammonia, Angew. Chem. Int. Ed. 58 (2019) 9464–9469.
[24] J. Wang, Y.P. Liu, H. Zhang, D.J. Huang, K. Chu, Ambient electrocatalytic nitrogen reduction on a MoO_2/graphene hybrid: experimental and DFT studies, Catal. Sci. Technol. 9 (2019) 4248–4254.
[25] X. Cheng, J.W. Wang, W. Xiong, T. Wang, T.W. Wu, S.Y. Lu, G. Chen, S.Y. Gao, X. F. Shi, Z.J. Jiang, X. Niu, X. Sun, Greatly enhanced electrocatalytic N_2 reduction over V_2O_3/C by P doping, ChemNanoMat 6 (2020) 1315–1319.
[26] Q. Qin, Y. Zhao, M. Schmallegger, T. Heil, J. Schmidt, R. Walczak, G. Gescheidt-Demner, H.J. Jiao, M. Oschatz, Enhanced electrocatalytic N_2 reduction via partial anion substitution in titanium oxide-carbon composites, Angew. Chem. Int. Ed. 58 (2019) 13101–13106.
[27] T. Xu, D.W. Ma, C.B. Li, Q. Liu, S.Y. Lu, A.M. Asiri, C. Yang, X.P. Sun, Ambient electrochemical NH_3 synthesis from N_2 and water enabled by ZrO_2 nanoparticles, Chem. Commun. 56 (2020) 3673–3676.
[28] T.W. Wu, H.T. Zhao, X.J. Zhu, Z. Xing, Q. Liu, T. Liu, S.Y. Gao, S.Y. Lu, G. Chen, A. M. Asiri, Y. Zhang, X. Sun, Identifying the origin of Ti^{3+} activity toward enhanced electrocatalytic N_2 reduction over TiO_2 nanoparticles modulated by mixed-valent copper, Adv. Mater. 32 (2020), 2000299.
[29] Y.P. Liu, Y.B. Li, D.J. Huang, H. Zhang, K. Chu, ZnO quantum dots coupled with graphene toward electrocatalytic N_2 reduction: experimental and DFT investigations, Chem. Eur. J. 25 (2019) 11933–11939.
[30] L. Xia, B.H. Li, Y. Zhang, R. Zhang, L. Ji, H.Y. Chen, G.W. Cui, H.G. Zheng, X. P. Sun, F. Xie, Q. Liu, Cr_2O_3 nanoparticle-reduced graphene oxide hybrid: a highly active electrocatalyst for N_2 reduction at ambient conditions, Inorg. Chem. 58 (2019) 2257–2260.
[31] X. Lv, F.Y. Wang, J. Du, Q. Liu, Y.S. Luo, S.Y. Lu, G. Chen, S.Y. Gao, B.Z. Zheng, X. P. Sun, Sn dendrites for electrocatalytic N_2 reduction to NH_3 under ambient conditions, Sustain. Energy Fuels 4 (2020) 4469–4472.
[32] L.L. Zhang, L.X. Ding, G.F. Chen, X.F. Yang, H.H. Wang, Ammonia synthesis under ambient conditions: selective electroreduction of dinitrogen to ammonia on black phosphorus nanosheets, Angew. Chem. Int. Ed. 58 (2019) 2612–2616.
[33] J.X. Zhao, B. Wang, Q. Zhou, H.B. Wang, X.H. Li, H.Y. Chen, Q. Wei, D. Wu, Y. L. Luo, J.M. You, F. Gong, X. Sun, Efficient electrohydrogenation of N_2 to NH_3 by oxidized carbon nanotubes under ambient conditions, Chem. Commun. 55 (2019) 4997–5000.
[34] W.B. Qiu, X.Y. Xie, J.D. Qiu, W.H. Fang, R.P. Liang, X. Ren, X.Q. Ji, G.W. Cui, A. M. Asiri, G.L. Cui, B. Tang, X. Sun, High-performance artificial nitrogen fixation at ambient conditions using a metal-free electrocatalyst, Nat. Commun. 9 (2018) 3485.
[35] X.J. Zhu, T.W. Wu, L. Ji, C.B. Li, T. Wang, S.H. Wen, S.Y. Gao, X.F. Shi, Y.L. Luo, Q.L. Peng, X. Sun, Ambient electrohydrogenation of N_2 for NH_3 synthesis on non-metal boron phosphide nanoparticles: the critical role of P in boosting the catalytic activity, J. Mater. Chem. A 7 (2019) 16117–16121.
[36] X.X. Zhang, T.W. Wu, H.B. Wang, R.B. Zhao, H.Y. Chen, T. Wang, P.P. Wei, Y. L. Luo, Y.N. Zhang, X.P. Sun, Boron nanosheet: an elemental two-dimensional (2D) material for ambient electrocatalytic N_2-to-NH_3 fixation in neutral media, ACS Catal. 9 (2019) 4609–4615.
[37] Y. Zhang, H.T. Du, Y.J. Ma, L. Ji, H.R. Guo, Z.Q. Tian, H.Y. Chen, H. Huang, G. W. Cui, A.M. Asiri, F. Qu, L. Chen, X. Sun, Hexagonal boron nitride nanosheet for effective ambient N_2 fixation to NH_3, Nano Res. 12 (2019) 919–924.
[38] C.Y. Ling, X.W. Bai, Y.X. Ouyang, A.J. Du, J.L. Wang, Single molybdenum atom anchored on N-doped carbon as a promising electrocatalyst for nitrogen reduction into ammonia at ambient conditions, J. Phys. Chem. C 122 (2018) 16842–16847.
[39] V. Jaccarino, R.G. Shulman, J.W. Stou, Nuclear magnetic resonance in paramagnetic iron group fluorides, Phys. Rev. 106 (1957) 602–603.
[40] B. Ma, H. Zhao, T. Li, Q. Liu, Y. Luo, C. Li, S. Lu, A.M. Asiri, D. Ma, X. Sun, Iron-group electrocatalysts for ambient nitrogen reduction reaction in aqueous media, Nano Res. 14 (2021) 555–569.
[41] G.F. Chen, S. Ren, L. Zhang, H. Cheng, Y. Luo, K. Zhu, L.X. Ding, H. Wang, Advances in electrocatalytic N_2 reduction–strategies to tackle the selectivity challenge, Small Methods 3 (2019), 1800337.
[42] G. Rostamikia, S. Maheshwari, M.J. Janik, Elementary kinetics of nitrogen electroreduction to ammonia on late transition metals, Catal. Sci. Technol. 9 (2019) 174–181.
[43] X. Cui, C. Tang, Q. Zhang, A review of electrocatalytic reduction of dinitrogen to ammonia under ambient conditions, Adv. Energy Mater. 8 (2018), 1800369.
[44] R. Manjunatha, A. Schechter, Electrochemical synthesis of ammonia using ruthenium–platinum alloy at ambient pressure and low temperature, Electrochem. Commun. 90 (2018) 96–100.
[45] R.D. Milton, S. Abdellaoui, N. Khadka, D.R. Dean, D. Leech, L.C. Seefeldt, S. D. Minteer, Nitrogenase bioelectrocatalysis: heterogeneous ammonia and hydrogen production by MoFe protein, Energy Environ. Sci. 9 (2016) 2550–2554.
[46] X. Yang, J. Nash, J. Anibal, M. Dunwell, S. Kattel, E. Stavitski, K. Attenkofer, J. G. Chen, Y. Yan, B. Xu, Mechanistic insights into electrochemical nitrogen reduction reaction on vanadium nitride nanoparticles, J. Am. Chem. Soc. 140 (2018) 13387–13391.
[47] R. Cai, S. Minteer, Nitrogenase bioelectrocatalysis: from understanding electron-transfer mechanisms to energy applications, ACS Energy Lett. 3 (2018) 2736–2742.
[48] C. Ling, Y. Ouyang, Q. Li, X. Bai, X. Mao, A. Du, J. Wang, A general two-step strategy–based high-throughput screening of single atom catalysts for nitrogen fixation, Small Methods 3 (2019), 1800376.
[49] X.F. Li, Q.K. Li, J. Cheng, L. Liu, Q. Yan, Y. Wu, X.H. Zhang, Z.Y. Wang, Q. Qiu, Y. Luo, Conversion of dinitrogen to ammonia by FeN_3-embedded graphene, J. Am. Chem. Soc. 138 (2016) 8706–8709.
[50] S. Hu, X. Chen, Q. Li, F. Li, Z. Fan, H. Wang, Y. Wang, B. Zheng, G. Wu, Fe^{3+} doping promoted N_2 photofixation ability of honeycombed graphitic carbon nitride: the experimental and density functional theory simulation analysis, Appl. Catal. B 201 (2017) 58–69.
[51] Z. Wei, Y. Zhang, S. Wang, C. Wang, J. Ma, Fe-doped phosphorene for the nitrogen reduction reaction, J. Mater. Chem. A 6 (2018) 13790.
[52] P.J. Kulesza, B. Rytelewska, I.A. Rutkowska, K. Sobkowicz, A. Chmielnicka, T. Chouki, S. Emin, Electroreduction of nitrogen to ammonia at iron catalytic sites generated at interfaces utilizing iron phosphides and heme-type complexes, ECS Trans. 109 (2022) 3–16.
[53] L. Ji, L. Li, X. Ji, Y. Zhang, S. Mou, T. Wu, Q. Liu, B. Li, X. Zhu, Y. Luo, X. Shi, A. M. Asiri, X. Sun, Highly selective electrochemical reduction of CO_2 to alcohols on an FeP nanoarray, Angew. Chem. Int. Ed. 59 (2020) 758–762.
[54] K.P. Singh, E.J. Bae, J.S. Yu, Fe-P: a new class of electroactive catalyst for oxygen reduction reaction, J. Am. Chem. Soc. 137 (2015) 3165–3168.
[55] D. Zeng, T. Zhou, W.J. Ong, M. Wu, X. Duan, W. Xu, Y. Chen, Y.A. Zhu, D.L. Peng, Sub-5 nm ultra-fine FeP nanodots as efficient Co-catalysts modified porous g-C_3N_4 for precious-metal-free photocatalytic hydrogen evolution under visible light, ACS Appl. Mater. Interfaces 11 (2019) 5651–5660.
[56] A. Yildiz, T. Chouki, A. Atli, M. Harb, S.W. Verbruggen, R. Ninakanti, S. Emin, Efficient iron phosphide catalyst as a counter electrode in dye-sensitized solar cells, ACS Appl. Energy Mater. 4 (2021) 10618–10626.
[57] Z. Wang, Y. Wang, J. Wang, W. Xiao, G. Xu, Z. Li, C. Dai, H. Zhang, Z. Wu, L. Wang, Microwave-assisted to decorate Ru onto Hollow-structured Fe-P spheres as efficient Electrocatalyst for hydrogen generation in wide pH range, Appl. Surf. Sci. 623 (2023), 157026.
[58] T. Sun, S. Li, T. Li, X. Chen, D. Xu, H.G. Wang, A Simple synthesis of Fe_2P nanoparticles encapsulated doped carbon nanotube as electrocatalysts for oxygen reduction reaction and zinc-air battery, Energy Technol. 10 (2022), 2100877.
[59] L. Qin, X. Yu, J. Li, S. Li, Y. Liu, P. Qian, J. Wang, S. Wang, H. Jin, New synthesis route of iron-based catalyst for electrochemical oxygen reduction reaction, Int. J. Electrochem. Sci. 15 (2020) 9168–9178.
[60] K.U.D. Calvinho, A.W. Alherz, K.M.K. Yap, A.B. Laursen, S. Hwang, Z.J.L. Bare, Z. Clifford, C.B. Musgrave, G.C. Dismukes, Surface hydrides on Fe_2P electrocatalyst reduce CO_2 at low overpotential: steering selectivity to ethylene glycol, J. Am. Chem. Soc. 143 (2021) 21275–21285.
[61] X. Li, W. Liu, M. Zhang, Y. Zhong, Z. Weng, Y. Mi, Y. Zhou, M. Li, J.J. Cha, Z. Tang, H. Jiang, X. Li, H. Wang, Strong metal-phosphide interactions in core-shell geometry for enhanced electrocatalysis, Nano Lett. 17 (2017) 2057–2063.
[62] S. Xu, H. Zhao, T. Li, J. Liang, S. Lu, G. Chen, S. Gao, A.M. Asiri, Q. Wu, X. Sun, Iron-based phosphides as electrocatalysts for the hydrogen evolution reaction: recent advances and future prospects, J. Mater. Chem. A 8 (2020) 19729–19745.
[63] H. Zhang, Y. Zhang, S. Liu, Preparation of trace Fe_2P modified N,P Co-doped carbon materials and their application to hydrogen peroxide detection, Electroanalysis 33 (2023) 831–837.
[64] F. Han, C. Zhang, J. Yang, G. Ma, K. He, X. Li, Well-dispersed and porous FeP@C nanoplates with stable and ultrafast lithium storage performance through conversion reaction mechanism, J. Mater. Chem. A 4 (2016) 12781–12789.
[65] B. Hu, J.Y. Yuan, J.Y. Tian, M. Wang, X. Wang, L. He, Z. Zhang, Z.W. Wang, C. S. Liu, Co/Fe-bimetallic organic framework-derived carbon-incorporated cobalt-ferric mixed metal phosphide as a highly efficient photocatalyst under visible light, J. Colloid Interface Sci. 531 (2018) 148–159.
[66] F. Wu, Z. Chen, H. Wu, F. Xiao, S. Du, C. He, Y. Wu, Z. Ren, *In situ* catalytic etching strategy promoted synthesis of carbon nanotube inlaid with ultrasmall FeP nanoparticles as efficient electrocatalyst for hydrogen evolution, ACS Sustain. Chem. Eng. 7 (2019) 12741–12749.
[67] X. Yang, L. Kang, C.J. Wang, F. Liu, Y. Chen, Electrochemical ammonia synthesis from nitrite assisted by *in situ* generated hydrogen atoms on a nickel phosphide catalyst, Chem. Commun. 57 (2021) 7176–7179.
[68] T. Liu, A. Li, C. Wang, W. Zhou, S. Liu, L. Guo, Interfacial electron transfer of Ni_2P–NiP_2 polymorphs inducing enhanced electrochemical properties, Adv. Mater. 30 (2018), 1803590.
[69] E.J. Popczun, J.R. McKone, C.G. Read, A.J. Biacchi, A.M. Wiltrout, N.S. Lewis, R. E. Schaak, Nanostructured nickel phosphide as an electrocatalyst for the hydrogen evolution reaction, J. Am. Chem. Soc. 135 (2013) 9267.
[70] E.J. Roberts, C.G. Read, N.S. Lewis, R.L. Brutchey, Phase directing ability of an ionic liquid solvent for the synthesis of HER-active Ni_2P nanocrystals, ACS Appl. Energy Mater. 1 (2018) 1823–1827.
[71] J. Wu, J.H. Li, Y.X. Yu, Highly stable Mo-doped Fe_2P and Fe_3P monolayers as low-onset-potential electrocatalysts for nitrogen fixation, Catal. Sci. Technol. 11 (2021) 1419.
[72] T. Chouki, M. Machreki, I.A. Rutkowska, B. Rytelewska, P.J. Kulesza, G. Tyuliev, M. Harb, L.M. Azofra, S. Emin, Highly active iron phosphide catalysts for selective electrochemical nitrate reduction to ammonia, J. Environ. Chem. Eng. 11 (2023), 109275.
[73] T. Chouki, M. Machreki, S. Emin, Solvothermal synthesis of iron phosphides and their application for efficient electrocatalytic hydrogen evolution, Int. J. Hydrog. Energy 45 (2020) 21473–21482.

[74] P. Liu, J.A. Rodriguez, Catalysts for hydrogen evolution from the [NiFe] hydrogenase to the ni$_2$P(001) surface: the importance of ensemble effect, J. Am. Chem. Soc. 127 (2005) 14871–14878.
[75] J.A. Rodriguez, P Liu, T. Asakura, J. Gomes, K. Nakamura, Desulfurization reactions on Ni_2P(001) and α-Mo_2C(001) surfaces: complex role of P and C sites, J. Phys. Chem. B 109 (2005) 4575–4583.
[76] B. Carlsson, M. Golin, S. Rundqvist, Determination of the homogeneity range and refinement of the crystal structure of Fe_2P, J. Solid State Chem. 8 (1973) 57.
[77] T. Gu, X. Wu, S. Qin, C. McCammon, L. Dubrovinsky, Probing nonequivalent sites in iron phosphide Fe_2P and its mechanism of phase transition, Eur. Phys. J. B 86 (2013) 311.
[78] P. Dera, B. Lavina, L.A. Borkowski, V.B. Prakapenka, S.R. Sutton, M.L. Rivers, R. T. Downs, N.Z. Boctor, C.T. Prewitt, High-pressure polymorphism of Fe_2P and its implications for meteorites and Earth's core, Geophys. Res. Lett. 35 (2008) L10301.
[79] G. Li, H. Lin, Z. Pan, Y. Liu, L. An, Boosting electrocatalytic nitrogen reduction to ammonia in alkaline media, Int. J. Energy Res. 45 (2021) 19634–19644.
[80] C.E. Housecroft, A.G. Sharpe, Inorganic Chemistry, 5th ed., Pearson, Harlow, UK, 2018.
[81] B.A. Lopez de Mishima, D. Lescano, T.M. Holgado, H.T. Mishima, Electrochemical oxidation of ammonia in alkaline solutions: its application to an amperometric sensor, Electrochim. Acta 43 (1998) 395–404.
[82] S. Trasatti, O.A. Petrii, Real surface area measurements in electrochemistry, Pure Appl. Chem. 63 (1991) 711–734.
[83] K. Vasquez, Ammonia Questions, 100, C&EN Global Enterprise, 2022, pp. 19–21.
[84] N. Ramaswamy, S. Mukerjee, Influence of inner- and outer-sphere electron transfer mechanisms during electrocatalysis of oxygen reduction in alkaline media, J. Phys. Chem. C 115 (2011) 18015–18026.
[85] V. Rosca, M.T.M. Koper, Electrocatalytic oxidation of hydrazine on platinum electrodes in alkaline solutions, Electrochim. Acta 53 (2008) 5199–5205.
[86] S. Wasmus, E.J. Vasini, M. Krausa, H.T. Mishima, W. Vielstich, DEMS-cyclic voltammetry investigation of the electrochemistry of nitrogen compounds in 0.5 M potassium hydroxide, Electrochim. Acta 39 (1994) 23–31.
[87] G.R. Medders, F. Paesani, Infrared and Raman spectroscopy of liquid water through "first-principles" many-body molecular dynamics, J. Chem. Theory Comput. 11 (2015) 1145–1154.
[88] M. Alinovi, G. Mucchetti, U. Andersen, T.A.M. Rovers, B. Mikkelsen, L. Wiking, M. Corredig, Applicability of confocal Raman microscopy to observe microstructural modifications of cream cheeses as influenced by freezing, Foods 9 (2020) 679.
[89] S. Xie, Y. Song, Z. Liu, *In situ* high-pressure study of ammonia borane by Raman and IR spectroscopy, Can. J. Chem. 87 (2009) 1235–1247.
[90] H.V.L. Nguyen, I. Gulaczyk, M. Kręglewski, I. Kleiner, Large amplitude inversion tunnelling motion in ammonia, methylamine, hydrazine, and secondary amines: from structure determination to coordination chemistry, Coord. Chem. Rev. 436 (2021), 213797.
[91] L.M. Malard, M.A. Pimenta, G. Dresselhaus, M.S. Dresselhaus, Raman spectroscopy in graphene, Phys. Rep. 473 (2009) 51–87.
[92] A.J. Bard, L.R Faulkner, Electrochemical Methods, VCH, New York, 1994.
[93] J. Deng, J.A. Iniguez, C. Liu, Electrocatalytic nitrogen reduction at low temperature, Joule 2 (2018) 846–856.
[94] T. Shinagawa, A.T. Garcia-Esparza, K. Takanabe, Insight on Tafel slopes from a microkinetic analysis of aqueous electrocatalysis for energy conversion, Sci. Rep. 5 (2015) 13801.
[95] A.R. Singh, B.A. Rohr, J.A. Schwalbe, M. Cargnello, K. Chan, T.F. Jaramillo, I. Chorkendorff, J.K. Norskov, Electrochemical ammonia synthesis-the selectivity challenge, ACS Catal. 7 (2017) 706–709.
[96] I.D. Raistrick, J.R. Macdonald, D.R. Franceschetti, Impedance Spectroscopy: Theory, Experiment, and Applications, Third ed., John Wiley and Sons, 2018, pp. 21–105.
[97] Z. Galus, Fundamentals of Electrochemical Analysis, Horwood, New York, 1994, 2nd Revised Ed.
[98] I.A. Rutkowska, P.J. Kulesza, Electroanalysis of ethanol oxidation and reactivity of platinum-ruthenium catalysts supported onto nanostructured titanium dioxide matrices, J. Electrochem. Soc. 163 (2016) H3052–H3060.
[99] W.B. Postek, I.A. Rutkowska, J.A. Cox, P.J. Kulesza, Electrocatalytic effects during redox reactions of arsenic at platinum nanoparticles in acid medium: possibility of preconcentration, electroactive film formation, and detection of As (III) and As(V), Electrochim. Acta 319 (2019) 499–510.
[100] M. Choi, M.H. Seo, H.J. Kim, E.J. Lim, W.B. Kim, Effect of polyoxometalate amount deposited on Pt/C electrocatalysts for CO tolerant electrooxidation of H_2 in polymer electrolyte fuel cells, Int. J. Hydrog. Energy 35 (2010) 6853.
[101] M. Heinen, Z. Jusys, R.J. Bhem, Ethanol, acetaldehyde and acetic acid adsorption/electrooxidation on a Pt thin film electrode under continuous electrolyte flow: an *in situ* ATR-FTIRS flow cell study, J. Phys. Chem. C 114 (2010) 9850.
[102] Y. Cao, P. Li, T. Wu, M. Liu, Y. Zhang, Electrocatalysis of N_2 to NH_3 by HKUST-1 with High NH_3 Yield, Chem. Asian J. 15 (2020) 1272–1276.
[103] Z. Weng, Y. Wu, M. Wang, J. Jiang, K. Yang, S. Huo, X.F. Wang, Q. Ma, G. W. Brudvig, V.S. Batista, Y. Liang, Z. Feng, H. Wang, Active sites of copper-complex catalytic materials for electrochemical carbon dioxide reduction, Nat. Commun. 9 (2018) 415.
[104] Y. Guo, H. Jin, Z. Qi, Z. Hu, H. Ji, L.J. Wan, Carbonized-MOF as a sulfur host for aluminum–sulfur batteries with enhanced capacity and cycling life, Adv. Funct. Mater. 29 (2019), 1807676.
[105] S.Z. Andersen, V. Čolić, S. Yang, J.A. Schwalbe, A.C. Nielander, J.M. Mcenaney, K. Enemark-Rasmussen, J.G. Baker, A.R. Singh, B.A. Rohr, M.J. Statt, S.J. Blair, S. Mezzavilla, J. Kibsgaard, P.C.K. Vesborg, M. Cargnello, S.F. Bent, T. F. Jaramillo, I.E.L. Stephens, J.K. Nørskov, I. Chorkendorff, A rigorous electrochemical ammonia synthesis protocol with quantitative isotope measurements, Nature 570 (2019) 504–508.
[106] X. He, Z. Ling, X. Peng, X. Yang, L. Ma, S. Lu, Facile synthesis of Cu_2SnS_3 nanocrystals for efficient nitrogen reduction reaction, Electrochem. Commun. 148 (2023), 107441.